JGR Solid Earth

RESEARCH ARTICLE
10.1029/2020JB020924

Lithospheric Structure and Flat-Slab Subduction in the Northern Appalachians: Evidence From Rayleigh Wave Tomography

Omid Bagherpur Mojaver[1], **Fiona Darbyshire**[1], **and Riddhi Dave**[1]

[1]Centre de recherche Geotop, Université du Québec à Montréal, Montréal, QC, Canada

Key Points:

- Lithospheric thicknesses and seismic velocities in eastern Canada are more variable in the Peri-Gondwanan than Peri-Laurentian domains
- Lithospheric thickness in the northern Appalachians varies in 70–120 km range and does not suggest a simple relation to the age of terranes
- The thicker lithosphere beneath New Brunswick may be caused by slab stacking resulting from flat subduction of Acadian lithosphere

Supporting Information:

- Supporting Information S1

Correspondence to:

O. Bagherpur Mojaver,
omid.bagherpur@gmail.com

Citation:

Bagherpur Mojaver, O., Darbyshire, F., & Dave, R. (2021). Lithospheric structure and flat-slab subduction in the northern Appalachians: Evidence from Rayleigh wave tomography. *Journal of Geophysical Research: Solid Earth*, *126*, e2020JB020924. https://doi.org/10.1029/2020JB020924

Received 4 SEP 2020
Accepted 4 MAR 2021

Abstract A billion years of tectonic history makes southeastern Canada and the northeastern United States an exciting area to investigate the evolution of continental lithosphere. Our study area comprises terranes with either Laurentian or Gondwanan provenance that accreted to eastern North America at different times. With the aim of resolving the isotropic velocity variations across the northern Phanerozoic Appalachians and the southeastern Proterozoic Grenville Province, we adopted a Rayleigh wave tomography technique that takes multipathing, scattering, and finite frequency effects into account. Our data sets include records of teleseismic earthquakes recorded by 71 broadband seismic stations over a 2-year period. Our high-resolution tomography models indicate significant (±3.5%) variations in shear wave velocity across different lithospheric domains, enabling us to discuss tectonic implications. In contrast to the Peri-Laurentian zones, seismic signatures in the Peri-Gondwanan domains are more complex and variable. Although systematic variations of seismic velocities across different tectonic zones are observed, we find no simple relation between the lithospheric thicknesses of different tectonic zones and their age. We interpret the lithosphere-asthenosphere boundary in our study area, located at 70–120 km depth, with the thickest and fastest lithosphere beneath New Brunswick. We suggest that this relatively thicker lithosphere is due to a slab stacking process that occurred after flat subduction of a younger domain in the Late Silurian. Occurrence of flat subduction in the Late Silurian in the northern Appalachians is also supported by geochemical and paleomagnetic evidence.

Plain Language Summary The lithosphere, the uppermost layer of the Earth, comprises a number of continental and oceanic blocks overlying a mechanically weaker and hotter layer. Our understanding of the formation and evolution of continental lithosphere is still incomplete. Southeastern Canada and the northeastern United States record a billion years of Earth history making this area an excellent region to investigate continental evolution. This motivated us to use a specialized technique in seismology, called Rayleigh wave tomography, to obtain models of the velocity structure beneath our study area at depths from 50 to 200 km. Our data sets include the records of global earthquakes recorded by seismic stations in the study area over a 2-year period. The resulting high-resolution tomography images suggest that lithospheric thickness in our study area is 70–120 km, and that more variability is observed beneath the later-accreting eastern domains than the older western domains. The thickest and fastest lithosphere is observed beneath New Brunswick, and we interpret this as resulting from a tectonic process called slab stacking. During this process, shallow subduction of a younger lithospheric block added new material to the base of the existing lithosphere. This interpretation is also supported by geochemical and paleomagnetic evidence.

1. Introduction

The complex tectonic history of eastern Canada and the northeastern United States provides an opportunity to investigate the evolution of continental lithosphere that has experienced multiple Wilson cycles in the last billion years. Our study area covers the Phanerozoic northern Appalachians in New England, Maine, and maritime Canada, as well as the southeastern part of the Proterozoic Grenville Province. Different tectonic zones in this area have formed and accreted at different times, and a detailed look at the seismic structure of the lithosphere is crucial to understand the past tectonic processes. The main focus of this study is to develop velocity structure models beneath the northern Appalachians and the transition to the SE Grenville Province, and discuss their tectonic implications. Although previous studies have significantly improved

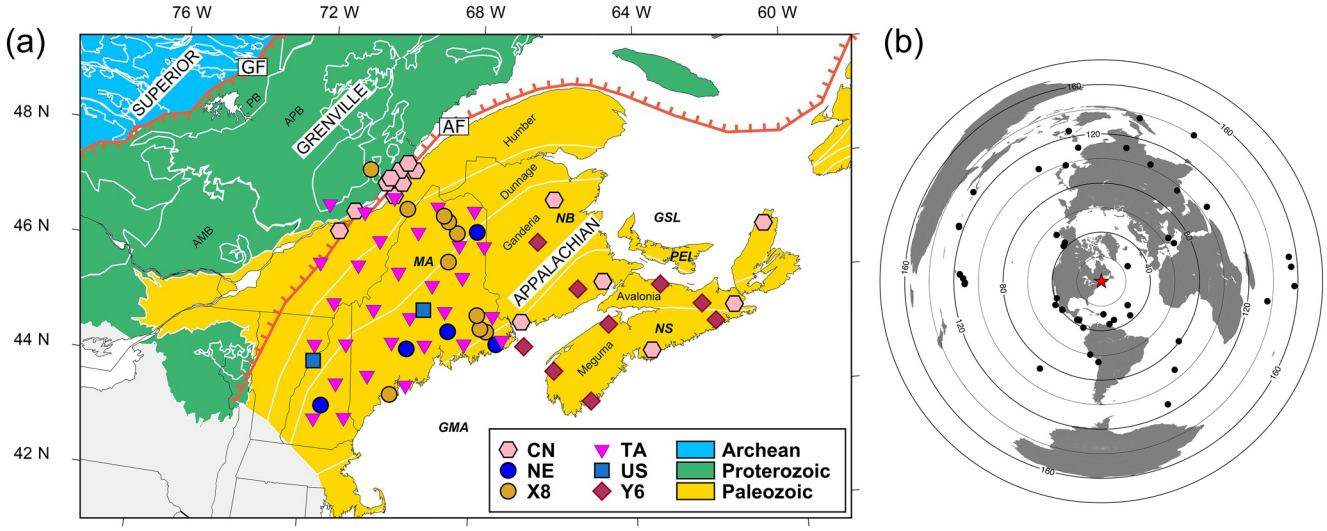

Figure 1. (a) The 71 broadband seismic stations belonging to six seismic networks overlain on a simplified tectonic map of the study area (station information in Table S1). Tectonic zones are separated by white lines. The Grenville Front (GF) and Appalachian Front (AF) are indicated by the red lines separating the major tectonic domains in eastern Canada. (b) Map of the 46 large earthquakes (black dots) used in this study (see also Table S2). The study area is marked by the red star. AMB, Allochthonous monocyclic belt; APB, Allochthonous polycyclic belt; GMA, Gulf of Maine; GSL, Gulf of Saint Lawrence; MA, Maine; NB, New Brunswick; NS, Nova Scotia; PEI, Prince Edward Island; PB, Parautochthonous belt.

our understanding of the tectonic history of the region, our understanding of the structure of this area and its tectonic evolution is still poor due to the limited resolution of previous models. Here, we take the most detailed look to date at the velocity structure of SE Canada and the NE United States using Rayleigh wave tomography applied to new data sets.

1.1. Tectonic Setting

Before the formation of supercontinent Pangea, a series of accretionary events in the early to late Paleozoic shaped the northern Appalachians. The Appalachian mountain belt is a ~485–350 Ma old orogen in eastern North America that has significantly deformed since its formation due to the protracted history of tectonic activities and erosion. The northern Appalachians extend from the New York promontory in the United States to Newfoundland in Canada, and evolved after a series of accretionary events related to amalgamation of Gondwanan-derived terranes to eastern Laurentia. These tectonic processes coincided with rift-drift processes during the opening and closure of the predecessors of the Atlantic ocean, the Iapetus and Rheic oceans (Hibbard et al., 2007a; van Staal et al., 2012).

Four orogenic episodes, the Taconic (485–450 Ma), Salinic (450–423 Ma), Acadian (421–400 Ma), and Neo-Acadian (395–350 Ma), contributed to the structure of the present-day northern Appalachians (van Staal et al., 2009, 2012; Levin et al., 2017). Based on geological properties, the northern Appalachians were divided into five tectonostratigraphic domains, namely Humber, Dunnage, Ganderia, Avalonia, and Meguma (Williams, 1979; Williams et al., 1988) (Figure 1a). It was later shown that the Humber and Dunnage zones were tectonized during the same orogenic episode: the Taconic orogeny (van Staal & Barr, 2012). The eastern domains, namely Ganderia, Avalonia, and Meguma, are categorized as the Appalachian Peri-Gondwanan realms (Hibbard et al., 2007a). These domains accreted to North America over three different orogenic episodes (van Staal et al., 2009, 2012).

The Humber zone extends along the entire northwestern edge of the Appalachians and records the history of the eastern Laurentian passive margin and a Taconic seaway (Hibbard et al., 2007b). Rift-related magmatism in this region is associated with the opening of the Taconic seaway and the Iapetus ocean at 615 Ma (Kamo et al., 1989). Geochronological evidence suggests that the Humber zone was active from Ordovician to Permian times (Karabinos et al., 2017). The Dunnage zone is composed of a set of continental and oceanic arc terranes that were situated in the Iapetus ocean and accreted to Laurentia in Ordovician times

(van Staal & Barr, 2012). The Dunnage zone comprises intra-oceanic terranes with either Gondwanan or Laurentian provenance that are separated by a faulting system named Red Indian Line (RIL; Macdonald et al., 2014; Williams et al., 1988). The location of RIL and its geometry at the subsurface, however, are still poorly constrained (Dorais et al., 2011).

Ganderia was rifted from the Amazonian margin of Gondwana in the late Neoproterozoic to early Cambrian (Wilson et al., 2017), and forms the basement of most of New Brunswick and Maine (Figure 1a). Accretion of Ganderia occurred in the late Ordovician to early Silurian marking the closure of the Iapetus ocean (van Staal et al., 2012). During the late Silurian to early Devonian Acadian orogeny, Avalonia was accreted to the eastern edge of Ganderia, culminating in the closure of the Acadian seaway (Wilson et al., 2017). The youngest accretionary event in the northern Appalachians occurred as Meguma accreted to eastern North America in the middle Devonian to early Carboniferous Neoacadian orogeny. Finally, the late-Paleozoic Alleghanian orogeny led to the final formation of the supercontinent Pangea. The northern Appalachians mostly escaped the deformation, metamorphism, and magmatism related to the Alleghanian orogeny (van Staal et al., 2012). Accordingly, structures arising from the accretionary events that occurred in the Paleozoic are very well preserved.

Our study area also covers part of the Proterozoic Grenville Province. This region records ~1 Ga of Earth history and is separated from the neighboring Appalachian orogen to the East by the Appalachian structural front. The Grenville orogeny was due to a ~100 Ma duration Himalayan-scale collision between Laurentia and Amazonia which culminated in the assembly of supercontinent Rodinia (e.g., Darbyshire et al., 2017; Hynes & Rivers, 2010; Whitmeyer & Karlstrom, 2007). Based on previous geophysical and geological studies, the Grenville Province is divided into three tectonic zones, including the Parautochthonous belt (PB), Allochthonous monocyclic belt (AMB), and Allochthonous polycyclic belt (APB) (Figure 1a). Our models cover eastern portions of the AMB and APB domains that include exotic terranes accreted during the Grenville orogeny, and contain rocks that metamorphosed during (and before) the orogenic cycle (Rivers et al., 1989).

1.2. Previous Seismic Studies

The seismic structure of the uppermost mantle in different parts of our study area has been investigated using different tomography techniques at different scales. Global and continental scale tomographic images do not show much variation of seismic velocities in the Appalachians, but a faster uppermost mantle structure in the Grenville Province is clearly evident (e.g., Boyce et al., 2019; Golos et al., 2018; Schaeffer & Lebedev, 2014; Yuan et al., 2014; Zhu et al., 2020). In comparison to a continental averaged global reference model, one can see elevated mantle seismic velocities at depths <150 km in both the Grenville Province and northern Appalachians (e.g., Schaeffer & Lebedev, 2014; Yuan et al., 2014). There are also a number of regional-scale lithospheric observations covering southeastern Canada and the northeastern United States with a relatively higher level of detail than continental-scale studies (e.g., Boyce et al., 2016; Petrescu et al., 2017; Villemaire et al., 2012). These regional-scale studies observe systematic variations of seismic velocities across the southeastern Grenville Province and the northern Appalachians, and also a faster recovered seismic structure in the Grenville Province than the younger northern Appalachian orogen.

The depth of the lithosphere-asthenosphere boundary (LAB) beneath our study area has been estimated to lie at 70–150 km depth by previous studies, using local-scale receiver function analysis (e.g., Rychert et al., 2005; Rychert & Shearer, 2009), continental- and global-scale surface wave tomography (e.g., Pasyanos et al., 2014; Priestley et al., 2018), joint inversions of body and surface wave data (e.g., Calò et al., 2016) and thermal modeling (e.g., Artemieva, 2006). We investigate lithospheric thickness variations at a higher resolution than previous studies, allowing us to interpret features on the scale of individual tectonic domains.

At crustal depths, easternmost Canada was previously studied during the Canadian Lithoprobe East (LE) project using seismic reflection-refraction methods (e.g., Hammer et al., 2010). Despite being beneficial for improving our understanding of the past tectonics, we note that caution must be taken in translating conclusions from the LE studies to our study area. This is due to the significant offsets between the terranes in Newfoundland and our study region caused by the irregular shape of the Laurentian margin before the Paleozoic accretionary events (Stockmal et al., 1987). According to the LE studies (e.g., Cook et al., 2010;

van der Velden et al., 2004), the Moho depths do not show a simple relation to the age of pertinent terranes, and crust is thinner beneath the central mobile belts in the Newfoundland Appalachians (~30–35 km) than the older easternmost Grenville (~40–45 km) and the younger Avalonia (~40 km). A northwest-dipping fabric at lower crust to mantle depths is imaged in central Newfoundland that likely indicates a relict subduction zone (e.g., van der Velden et al., 2004). Further west, upper- to mid-crustal depths beneath the Gulf of Saint Lawrence were studied using a surface wave tomography method, and westward dipping of Avalonia beneath Ganderia was interpreted (Kuponiyi et al., 2017). Continental-scale seismic tomography models at crustal depths show an overall decrease of seismic velocities from the eastern Grenville to the northern Appalachians but lack enough resolution to provide more detailed tectonic interpretations (e.g., Kao et al., 2013).

Until recently, sparse data coverage in easternmost Canada has limited resolution of lithospheric structure beneath the northeastern Appalachians. This has made it challenging to investigate variations of seismic wave speeds and LAB depths across the different tectonic zones. Having access to denser seismic networks than previous studies allows us to develop a high-resolution seismic velocity model that distinguishes lithospheric structural variation between the different tectonic zones of the northern Appalachians, as well as the nature of the transition from the lithosphere of the older Grenville Province.

2. Data and Data Processing

The data used in this study are fundamental-mode Rayleigh wavetrains recorded by 71 broadband seismic stations belonging to six different seismic networks, including the Canadian National Seismograph Network (CN; Geological Survey of Canada, 1989), New England Seismic Network (NE; ASL, 1994), USArray Transportable Array (TA; IRIS Transportable Array, 2003), United States National Seismic Network (US; ASL/USGS, 1990), and the QM-III experiment (X8 and Y8 networks; Menke et al., 2012; SEIS-UK, 2013) (Figure 1a). The stations belonging to the TA and QM-III networks operated between summer 2013 and summer 2015 and comprised ~70% of our data sets. We selected earthquakes of magnitude larger than 6 occurring between 2013 and 2015 with epicentral distances ranging from 20° to 160°. A total number of 46 events were selected (out of more than 300 events) based on azimuthal distribution, visual inspection of the frequency content of waveforms (dispersion quality), and signal-to-noise ratio (SNR) for extracting clear wavetrains to input to the tomography approach (Figure 1b).

Single station data processing procedure includes instrument response correction to a common sensor type (CMG-3T), event synchronization, resampling of the time-series, windowing, bandpass filtering, and final quality control. Time series were synchronized and decimated to a common sampling rate of 1 Hz for consistency. The selected seismograms were windowed to isolate the Rayleigh wavetrains and then filtered at 18 frequency bands with the central period ranging from 20 to 167 s, using a 10 mHz width, fourth-order, double-pass Butterworth filter (Figure 2). Finally, all seismograms were visually checked for the SNR and dispersion quality. Earthquake-station ray paths have excellent density and azimuthal coverage across our study area, with between 1079 and 2251 crossing rays at each period (Figure 3).

3. Methodology

Once Rayleigh wavetrains were extracted from the processed teleseismic data, the frequency-dependent characteristics of the wavetrains were studied in a Rayleigh wave tomography approach to obtain phase velocity variations. During their propagation along the source-receiver path, surface waves encounter many seismic heterogeneities and may pass through major tectonic boundaries, causing undesirable effects in the seismic records such as multipathing and scattering (e.g., Li & Fu, 2020). In traditional seismic tomography techniques, where surface wavetrains are considered as single plane waves, multipathing and scattering effects are not taken into account, causing bias in the measurements of surface wave characteristics as they traverse a seismograph network. In this study, we use the two-plane-wave tomography (TPWT) method (Forsyth et al., 1998; Forsyth & Li, 2005) that was developed to account for the nonplanar energy caused by those effects. In this method, the incoming wavefield is assumed to consist of two interfering plane waves with different amplitudes, phases, and propagation directions. As discussed by previous authors (e.g., Li & Li, 2015; Li, 2011; Yang & Forsyth, 2006), this formulation can reduce the misfit between the observed

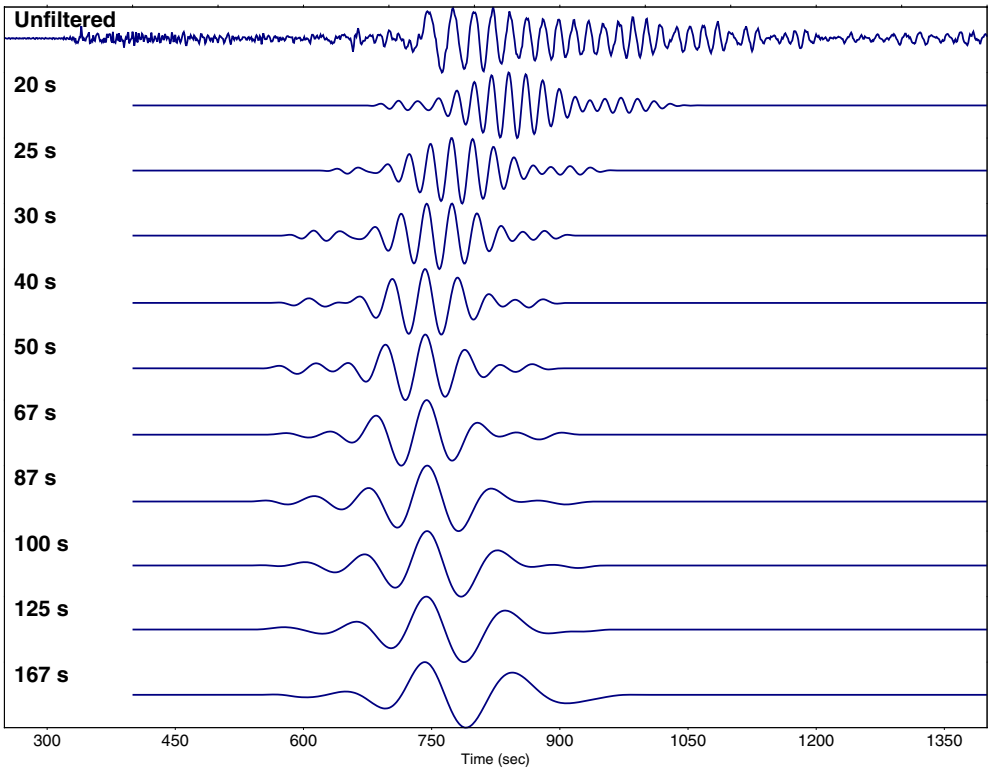

Figure 2. Example of data filtering for a $M_w = 6.1$ earthquake that occurred on July 27, 2014, on the northern mid-Atlantic ridge and recorded by CN.CHEG station in Nova Scotia. A subset of the 18 passbands used in this study is shown here.

and calculated wave parameters, and increase the resolution of the resulting phase velocity maps. The motivation to adopt the TPWT method came from the need to accurately resolve seismic structure under a densely spaced seismograph network while removing the scattering and multipathing effects. Unlike the two-station method, also commonly used in regional surface wave tomography, TPWT does not rely on great-circle-path alignments with pairs of stations, allowing a more flexible approach to azimuthal coverage for the events used in the analysis. In addition, the dense station spacing and the network aperture in our study area would lead to limitations in resolution at long periods due to the relatively short maximum inter-station distances; this is not an issue in TPWT.

In the forward problem setting, a local coordinate system is defined for each event with + x-direction along the great-circle path, and the observed amplitude and phase data are normalized relative to a reference station (Figure S9). The inverse problem comprises two steps that are repeated several times to ensure

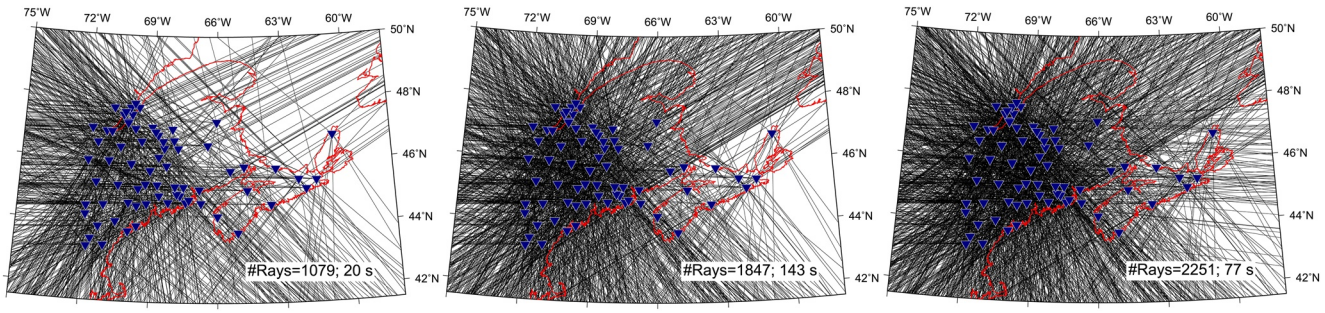

Figure 3. Ray path coverage at 20 s (left; lowest coverage), 143 s (middle; average coverage), and 77 s (right; best coverage). Seismic stations are indicated by blue triangles.

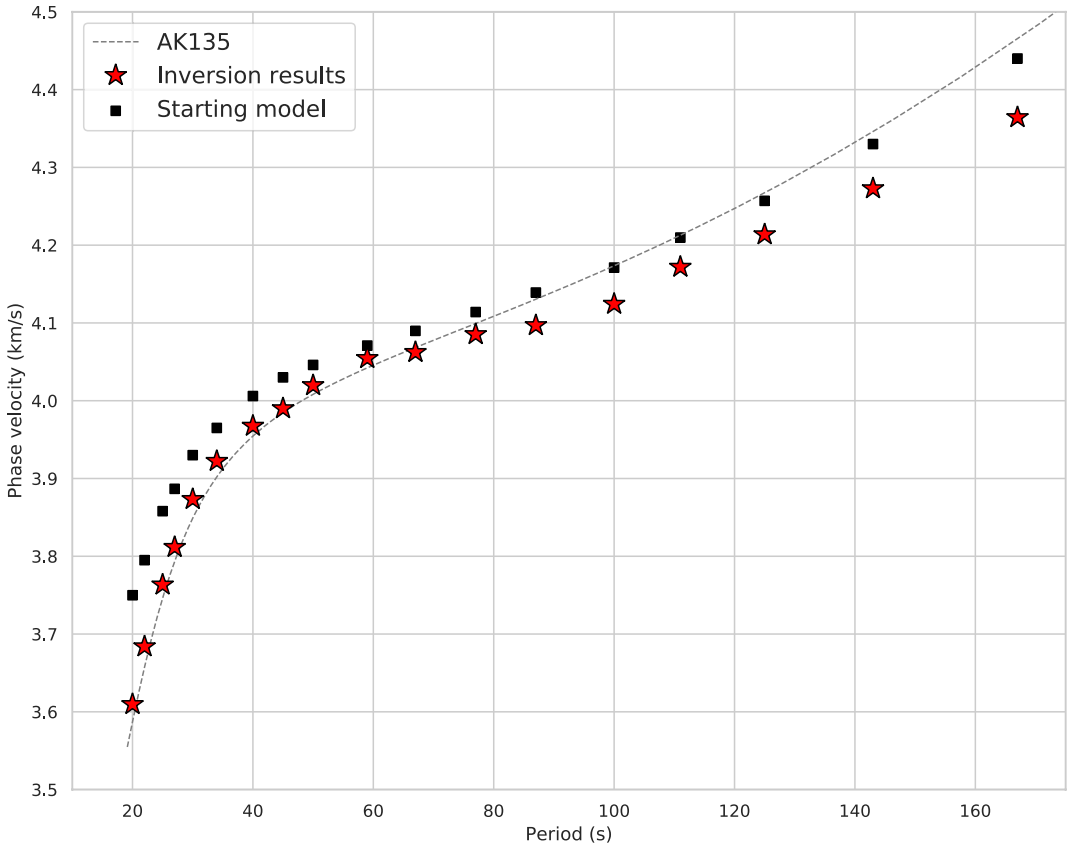

Figure 4. The average phase velocity dispersion curve resulting from the 1D TPWT. The starting model was obtained from forward modeling on a shear wave velocity profile extracted from the SL2013NA model of Schaeffer and Lebedev (2014).

that convergence criteria are met (Forsyth & Li, 2005). In the first step, the two plane wave parameters are estimated for each event using a probabilistic optimization technique. The resulting two plane wave parameters, along with the unknown model parameters (phase velocities over a grid), are jointly inverted using a linearized inversion method in the second step. Events that are poorly represented by the two-plane wave assumption are automatically down-weighted in this iterative joint inversion procedure. In contrast to the traditional tomography methods in which the horizontal sensitivity of plane waves is calculated using approximate Gaussian sensitivity functions, TPWT uses the more accurate 2D Born sensitivity kernels that take finite frequency effects into account (Figure S11; Zhou et al., 2004). This formalism improves model resolution over longer periods (Li, 2011; Li & Burke, 2006; Yang & Forsyth, 2006). Further details of the method are given in the supporting information.

In general, three input types are required in the TPWT procedure: (1) A starting model that roughly represents the regional average phase velocities at different periods, (2) a grid of nodes that parameterizes the study area, and (3) phase and amplitude data that can be obtained by applying a Fourier transform to the processed Rayleigh wavetrains. The starting model can be inferred from available tomography models covering the study area. Accordingly, we extracted a shear wave velocity profile at the center of the study area from the continental-scale shear wave velocity model SL2013NA (Schaeffer & Lebedev, 2014), and carried out forward modeling using the *SURF96* program (Herrmann, 2013). The resulting phase velocity dispersion curve was used as the initial model to input the 1D TPWT inversion to estimate the regional average Rayleigh wave phase velocity dispersion curve (Figure 4). This regionally averaged dispersion curve was later used as the starting model for the 2D TPWT inversions to map phase velocity variations across the study area at different periods.

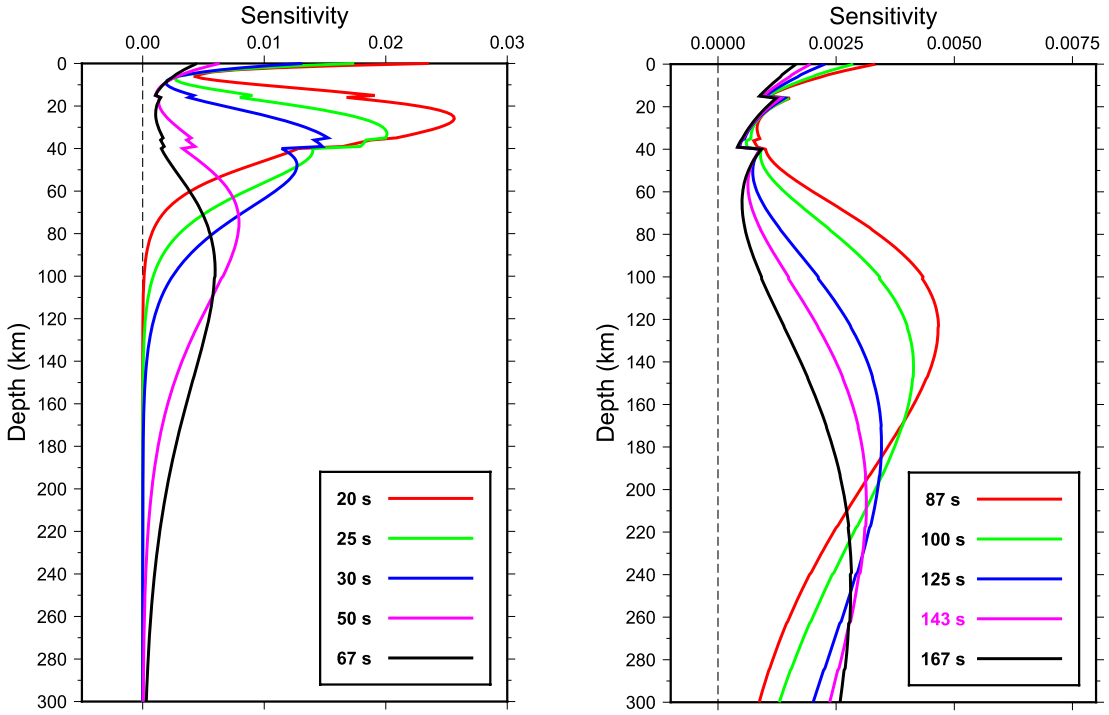

Figure 5. Depth sensitivity kernels for Rayleigh wave phase velocity at different periods. (Left) Short to intermediate periods that are most sensitive to lithospheric depths. (Right) Long periods that mostly sample lower lithosphere down to asthenospheric depths.

The periods measured in our study sample a depth range from the lower crust to the sublithospheric mantle (Rayleigh wave depth sensitivity kernels are shown in Figure 5). We invert our phase velocity models for shear wave velocity as a function of depth, using the *Shearsaito* program (after Saito, 1988). This is a linearized inversion technique that calculates 1D Earth structure using normal-mode formulations.

3.1. Inversion Setting

3.1.1. TPWT Inversion

In the TPWT inversions, we parameterized the study area, covering 41°N to 50°N, and 75°W to 57°W, into 475 uniformly spaced nodes separated by 0.75° × 0.5° along the longitude and latitude respectively. This region is slightly larger than the station coverage, reflecting the ray path distribution in the study area (Figure 3). Uniform spacing parameterization in TPWT has been applied to regions with nonuniform station spacing with great success in previous studies beneath different regions, including Iceland (Li & Detrick, 2006), South Africa (Li & Burke, 2006), Tanzania (Adams et al., 2012; O'Donnell et al., 2013; Weeraratne et al., 2003), and Tibet (L. Li et al., 2013). The edge nodes were 10 times more weakly damped as compared to the inner nodes (a priori error of 2 km/s vs. 0.2 km/s) to allow for the absorption of nonplanar energies which cannot be represented by the two-plane-wave assumption within the inner nodes (e.g., Chen & Li, 2012; A. Li et al., 2003). We use a characteristic length of 80 km for all frequencies to smooth the phase velocity models (Yang & Forsyth, 2006). This controls the weighting of a grid by its distance to each path in calculating slowness and travel times along the path. Our station spacing is comparable to the station spacing in A. Li et al. (2003), and their tests of characteristic length justify our choice of smoothing value. A smaller characteristic length would produce more smaller-scale variations in phase velocity models but would increase the variance on model parameters (A. Li et al., 2003), thus causing overfitting of the data. Tests of different inversion settings are available in Figure S1.

TPWT inversions also output the covariance matrix that can be used to extract information about uncertainties. We used the gridded variance data, extracted from the covariance matrix, to analyze and plot the standard error distribution maps. Considering the 1D average phase velocities resulting from the 1D TPWT,

we calculated the 2× standard error at all periods and chose the contour of 1.5% at 67 s as a proxy to mask out the maps outside this contour (hereafter, we call the region inside this contour the "confidence area"; error maps at other periods are also available in Figure S2). In theory, if we assume a Gaussian error distribution for the phase velocity solution, we should be able to resolve any anomaly of ±1.5% from the average at a 95% level of confidence within this contour. It should be noted that since this theoretical confidence area usually gets smaller at longer periods, it is better to exercise caution in giving interpretation for deep velocity anomalies closer to the edge regions.

3.1.2. Inversion for Shear Wave Velocity Structure

Having recovered the phase velocity model, we obtain shear wave velocity variations using the *Shearsaito* program. We first inverted the 1D average Rayleigh wave phase velocity dispersion curve for the 1D average shear wave velocity profile. Next, we interpolated the phase velocity maps with a denser grid spacing (0.1 × 0.1°) before extraction of dispersion curves to input to the *Shearsaito* inversions. Hence, more than 8,500 dispersion curves within an area slightly larger than the confidence area were extracted from the finely gridded phase velocity maps, and later inverted to build our (pseudo) 3D shear wave velocity model. In the majority of cases, the inversion results matched the dispersion data very well. However, at some edge areas where the errors were higher, especially at longer periods, the method tended to keep the model fairly close to the initial model, at the expense of fitting the longest period data.

We chose to use the AK135 global reference model (Kennett et al., 1995) as the basis for building our layered starting model as this model has a comparable crustal thickness to the average of our study area and smooth velocity profiles throughout the depth range of interest. We tested different starting model parameterizations and finally designed a starting model that was parameterized as three crustal layers with a Moho depth of 35 km, a stack of 10 km thick layers down to a depth of ~400 km, and increasing thickness of layers to maximum 50 km down to the base of the lower mantle. The crustal thickness and velocities at all layers down to 400 km depth were allowed to vary, and velocities at the deeper depths were fixed to the starting model. Since the inversion is forced to output a three-layer model for the crust, we were able to extract crustal thickness variations by calculating the summation of the thicknesses of the first three layers from the inversion outputs.

For the *Shearsaito* inversion settings, we tested several regularization parameters to find the best combination for data fit and model complexity (see Figure S3). A more weakly damped shear wave velocity solution for the 3D solution compared to the inversion of 1D average dispersion data was necessary. This is because the data errors extracted from the phase velocity maps and used in the pseudo-3D inversions are relatively larger. For the crustal thickness solution, a priori standard error of 10 km was chosen in both 1D and 3D inversions, allowing the inversion to explore a range comparable to that of the Moho depth variations across the region. A constant Vp/Vs ratio of $\sqrt{3}$, a standard value used for continental lithosphere, was used to calculate the inversion sensitivity kernels. Finally, to get velocity values at all depths rather than having a layered model, we performed linear interpolation with a depth interval of 1 km to all resulting layered shear wave velocity profiles.

4. Model Resolution

To examine the resolution of our phase velocity maps, we performed checkerboard resolution tests with different checkerboard cell sizes and various ranges of perturbations. Synthetic amplitudes and phases of Rayleigh waves were computed from the checkerboard model using the same stations, events, and ray paths as in the real data. These synthetic data were used to calculate 2D phase velocity using the same inversion technique as was used for the real data.

Here, we only show the checkerboard cell sizes that are compatible with the sizes of anomalies that we expect to image. Readers are referred to the supporting information for extra checkerboard resolution tests (Figures S4–S6). Accordingly, we chose a 3×3 grid node spacing cell size (2.25° × 1.5 °) that represents ~160 km × 160 km anomalous features. The range of phase velocity perturbations from the regional average at all periods was set to ±3.5% (Figure 6). The resolution test maps are clipped using the same confidence area

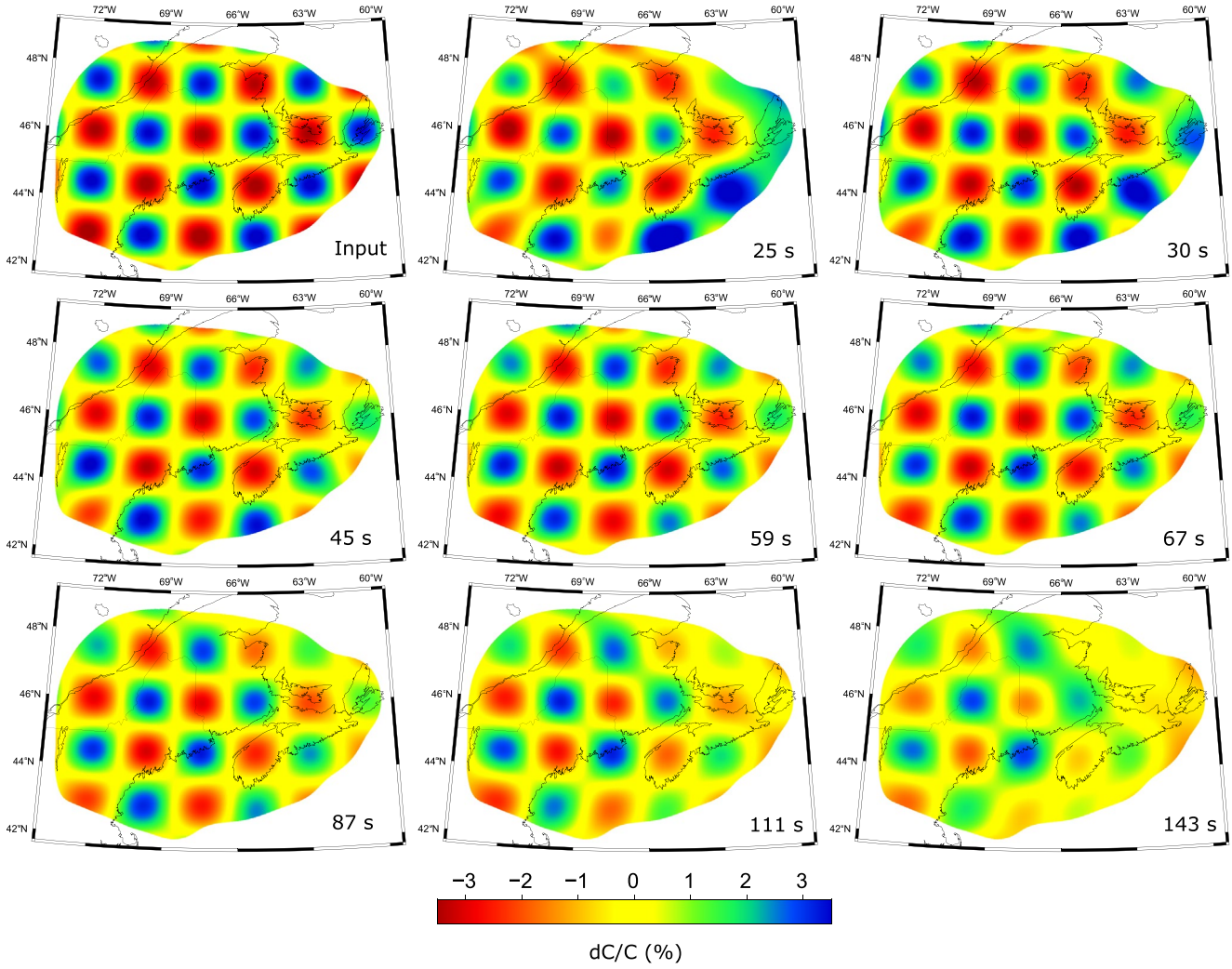

Figure 6. Checkerboard resolution tests of the phase velocity maps at different periods. The checkerboard cell size is 2.25° × 1.5°, and maps are clipped using the same confidence area that was used to clip phase velocity maps.

as we used to clip the phase velocity maps. Overall, the resolution analysis of the phase velocity maps shows good recovery of velocity anomalies at about 160 km × 160 km scale. Some smearing effects, especially at edge areas, are visible at the shortest and longest periods indicating that the geometry of the structure at these areas and depths sensitive to the corresponding periods are not well resolved. Amplitude recovery of anomalies is imperfect due to regularization effects and ray coverage variations. The effect is generally period-dependent, but can also be affected by the strength of the original anomaly (e.g., A. Li et al., 2003, Figures 6, S5, and S6). We use these results to guide our model interpretations.

5. Results

5.1. Phase Velocities

The initial step in TPWT analysis is the calculation of a dispersion curve that represents the average 1D structure across the entire study region. The resulting 1D average Rayleigh wave phase velocity model covers periods from 20 to 167 s and has been smoothed using Gaussian sensitivity functions. This regional average phase velocity dispersion curve is in good agreement with the predictions from both the global reference (continental) AK135 model and our starting model (Schaeffer & Lebedev, 2014). We observe a close agreement with the AK135 model at periods shorter than ~67 s, with lower velocity values in our model at

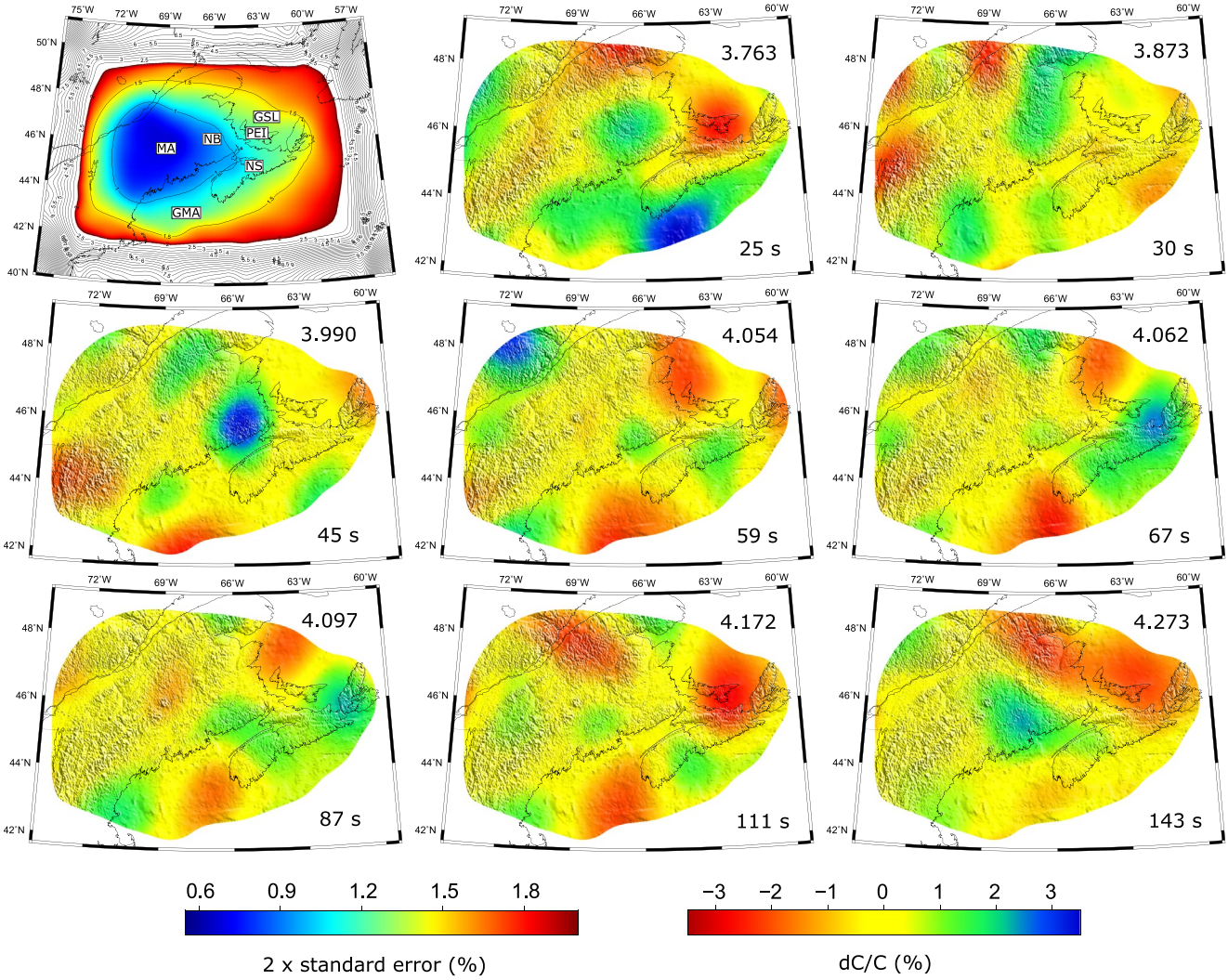

Figure 7. Maps of phase velocity variations across the study area. Velocities are given in terms of perturbations from the 1D average phase velocities that were obtained in the previous step, and these background values (in km/s) are shown at the upper right corner of all maps. The 2× standard error distribution map at 67 s is shown in the top left panel. The contour of 1.5% on this map was chosen as the confidence area to clip the results. GMA, Gulf of Maine; GSL, Gulf of Saint Lawrence; MA, Maine; NB, New Brunswick; NS, Nova Scotia; PEI, Prince Edward Island. See Supporting Information for phase velocities and the error distribution maps at other periods (Figures S2, S7, and S8).

longer periods (Figure 4). This should result in a similar average shear wave velocity profile at lithospheric depths overlying lower velocities at asthenospheric depths. The standard deviation of estimates increases with period and ranges from 0.002 to 0.014 km/s. Such small uncertainties are due to the excellent ray path coverage provided by our data sets. Although these theoretical error values might not reflect data measurement uncertainties, they can be considered as a tool to compare errors at different periods.

We present the phase velocity maps in terms of perturbations from the 1D average phase velocities that we obtained in the previous step (Figures 7, S7, and S8). Our phase velocity maps show the variation of phase velocity on a ±3.5%–4% scale across the study area. In general, anomalies have a northeast-southwest trend that is parallel to the Appalachian trend. Correlation of phase velocity anomalies at adjacent periods is observed, especially at longer periods, that are due to overlaps of depth sensitivity kernels to the Earth structure (Figure 5). The observed consistency of features at adjacent periods suggests that these anomalies are real features. Examples include the low-velocity zones at periods longer than 45 s in the Gulf of Saint Lawrence (GSL) and the Gulf of Maine (GMA) (Figure 7).

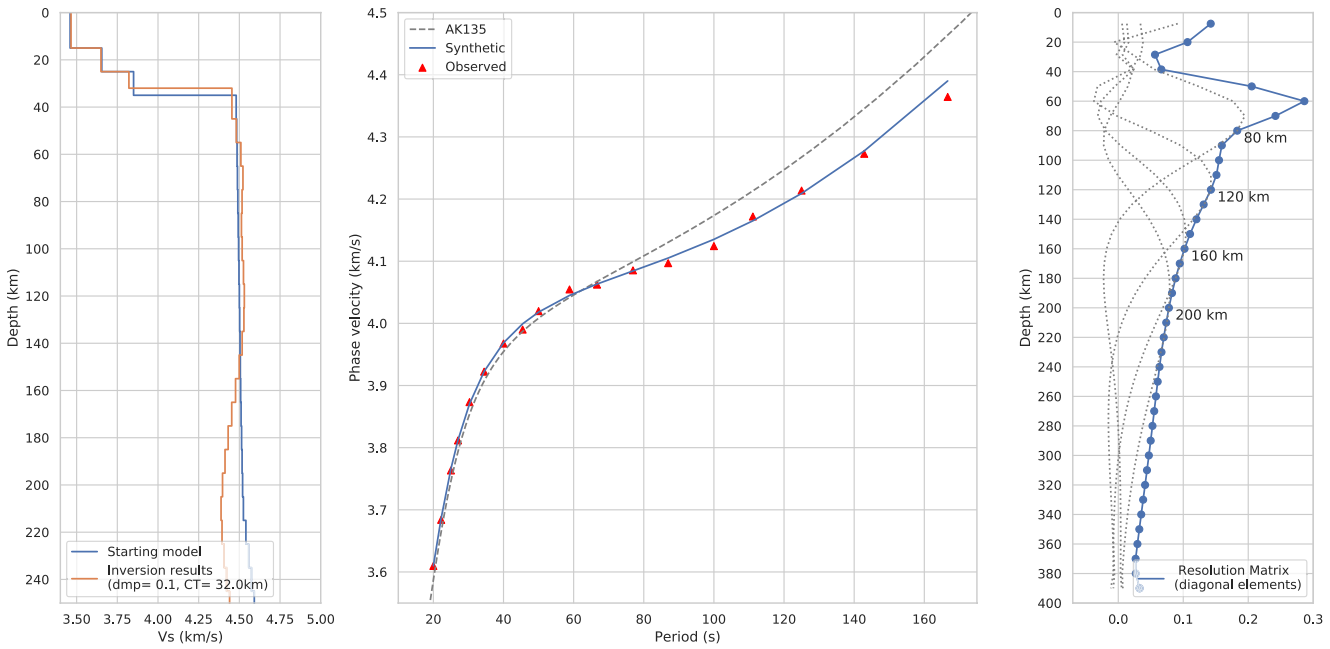

Figure 8. Linearized inversion results for the 1D average shear wave velocity. (Left) Shear wave velocity profile. (Middle) Synthetic and observed dispersion curves. (Right) Resolution matrix profiles.

In summary, the phase velocity maps at periods sensitive to lithospheric structures show the greatest variability in phase velocities. The phase velocity perturbations at the shortest periods (<40 s) suggest lateral variations in the deep crustal structure and around the Moho on a ±3.5–4% scale. The most notable features at this period range are the low-velocity anomalies aligned with geological strike (NE-SW) beneath the Humber and Dunnage zones, and also beneath the GSL. Notable high-velocity anomalies at these periods are seen in the southeast of the study area, beneath the GMA. Phase velocities at a period range from 20 to 27 s are sensitive to lower crustal structures, and they show features with largest perturbations from the average, indicating the complexity of crustal structure across the study area. Maps at periods between 30 and 34 s have their maximum sensitivity around the Moho depth, and therefore could indicate variations in the crustal thickness. At those periods, positive anomalies are observed in the GMA and in New Brunswick. On the other hand, the most negative anomalies are recovered in the Peri-Laurentian domains.

At the intermediate period range (40–87 s), phase velocities are sensitive to lithospheric mantle structures. Perturbations of phase velocities at these periods show variations in the ±3% range. At these periods, phase velocity variations could be interpreted as variations of temperature and composition in the lithosphere as well as lithospheric thickness across the study area. The most prominent anomalies in this period range include high-velocity anomalies in the Grenville Province, Nova Scotia, and New Brunswick, whereas negative velocity anomalies are observed in the GSL, GMA, and southwestern parts of the study area. At the longest periods (100–167 s), our phase velocity model still shows considerable variations (±2.5%). Prominent negative anomalies (maximum −2.5% perturbation from the global reference) at these periods are observed beneath northern Maine, northern New Brunswick, the GSL, and the GMA. Beneath southern Maine and southern New Brunswick, positive anomalies reach a peak of +2.5%, whereas southern Nova Scotia and the southwest of the study area are underlain by positive anomalies up to +1.5%.

5.2. Shear Wave Structure

The obtained 1D shear wave model of our study area agrees well with the predictions from the AK135 global reference model down to a depth of ~140 km, with velocities slower than AK135 below this depth (Figure 8). The inversion results also suggest an average crustal thickness of 32 km beneath the study area. In the 3D model, the systematic variation in crustal thickness observed between tectonic domains is similar to that inferred from receiver function analyses (Figure 9). However, our model cannot reproduce the same

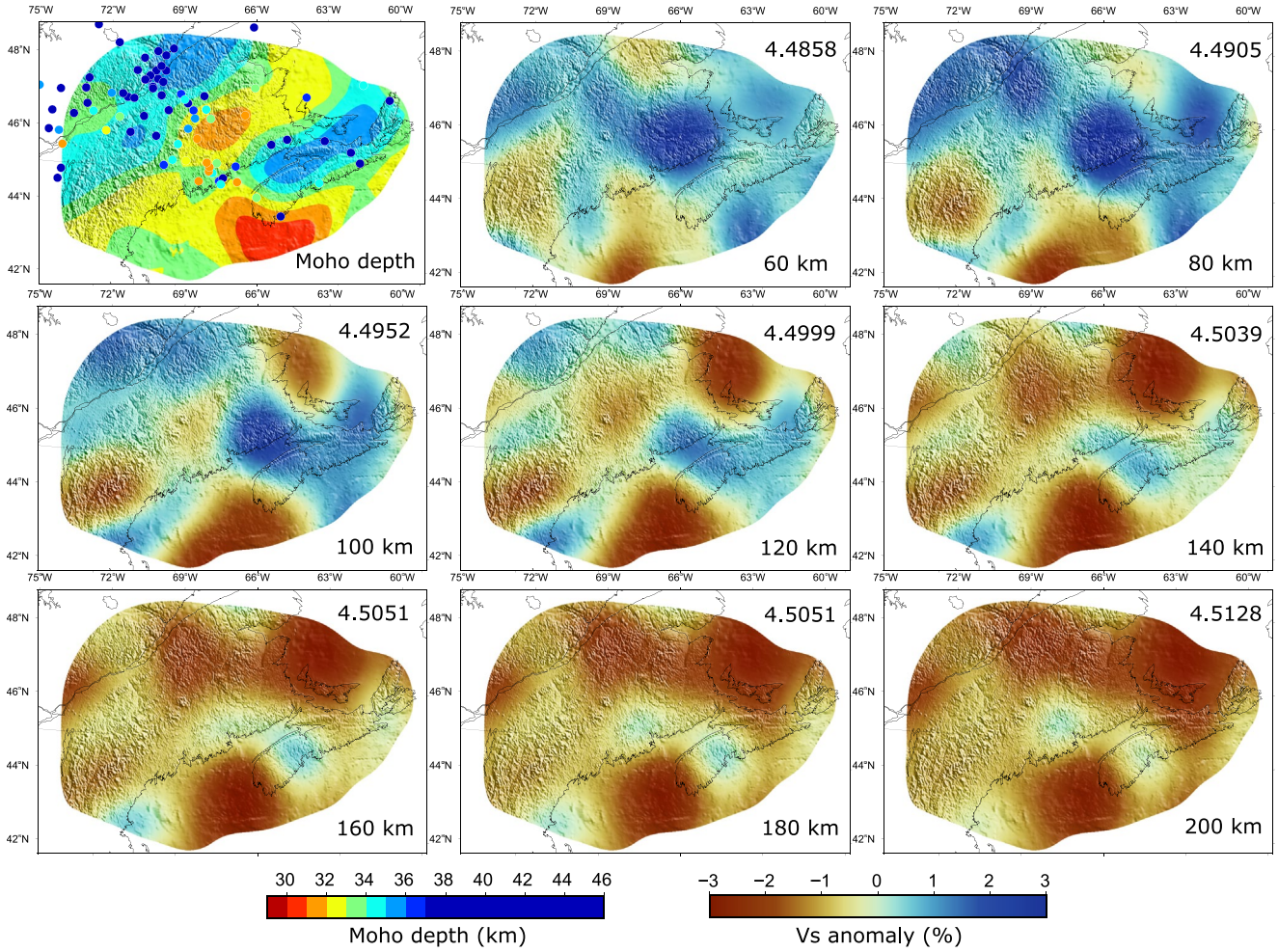

Figure 9. Maps of shear wave velocity variations and the recovered Moho depth model (upper left). Shear wave velocities are given in terms of perturbations from the linearly interpolated continental AK135 reference model, and the background values (in km/s) are marked at the upper right corner of each map. The compilation of receiver function results from Darbyshire et al. (2017) is overlaid on the Moho depth map (colored circles).

absolute values of Moho depth, due to the intrinsic differences in the methods and the trade-offs in the inversion between lower-crustal velocity, Moho depth, and velocity in the layer immediately below the Moho. Given these trade-offs, as well as information from the resolution matrix profiles (Figure 8, right panel), we interpret the modeled shear wave velocity variations for upper-mantle depths only, over a 50–200 km depth range. We restrict our interpretations of crustal structure to those of relative crustal thicknesses across the study region, which we consider to be robust.

The highest velocity anomalies are observed in the 50–120 km depth range in the Peri-Laurentian domains, New Brunswick and Nova Scotia. The fast velocity anomaly in the Peri-Laurentian domains (Grenville, Humber, and western Dunnage) clearly distinguishes these regions from Peri-Gondwanan domains down to a depth of ~100 km. In addition, our modeling results show a relatively thicker crust in the majority of these areas. The most prominent high-velocity anomaly in our region is observable in New Brunswick. This anomaly shows 1.5%–3% perturbations from the reference model down to ~120 km depth. Another strong high-velocity anomaly is observed in Nova Scotia, showing maximum perturbations of ~1.5%–2% down to the depth of 100 km. We also observe a relatively small high-velocity anomaly in the southwest of the study region at the margin of the clipped area on the coastline. This anomaly is clearly observable at depths of < 140 km (Figure 9). Although this marginal positive anomaly is relatively smaller and weaker than other observed positive anomalies, it is likely to suggest a different lithotectonic unit than its neighboring slow regions.

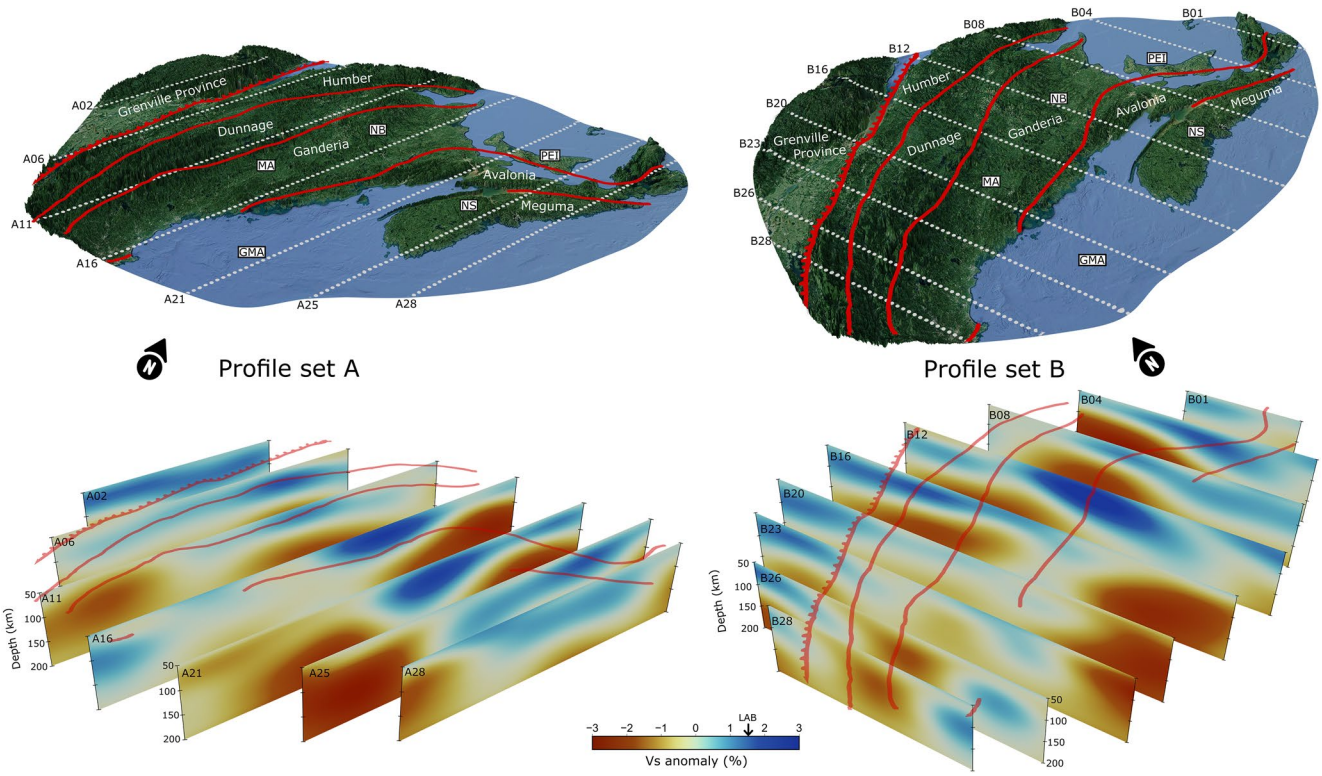

Figure 10. Cross-sections of the recovered shear wave velocity structure from different viewing angles. Top figures show the tectonic boundaries (red lines) and the corresponding tracks (white lines) of the cross-sections shown in the bottom figures. All cross-sections and topography maps were clipped using the confidence area. The label "LAB" on the color scale marks the proxy value used to locate the lithosphere-asthenosphere boundary. GMA, Gulf of Maine; MA, Maine; NB, New Brunswick; NS, Nova Scotia; PEI, Prince Edward Island.

We observe negative anomalies in our shear wave velocity model beneath the GMA, GSL, northern New Brunswick and Maine, and the southwest of the study area. The slow velocity anomaly observed beneath the GMA is a strong 2%–3% negative anomaly that exists at a wide range of depths (60–200 km). A prominent low-velocity anomaly is also observed beneath the GSL. This negative anomaly is clearly visible from 100 km depth, and shows perturbations from AK135 in the 1.5%–3% range. At 100–120 km depth, our shear wave velocity model indicates a velocity contrast of > 3% between the northwest and southeast of GSL. Further south, a slow anomaly is observed beneath northern New Brunswick and Maine, with velocities 1%–3% slower than the global reference. This anomaly is evident in our model from 120 km depth and continues to expand and get stronger toward the Appalachian Front to the north. We also observe a low-velocity zone beneath the southwestern part of the study area, with maximum perturbations of ~2% between 70 and 130 km depth.

6. Discussion

6.1. Seismic Signatures of the Tectonic Domains

To date, our models offer the most detailed look at the isotropic velocity structure of the northern Appalachians and the southeastern Grenville Province. The maps from our velocity models show a dominant NE-SW trend in anomalies, consistent with the strike of the tectonic domains in the region (Figures 7 and 9). Elevated velocities in the Peri-Laurentian domains (Grenville, Humber zone, and the western parts of the Dunnage zone) and beneath the post-Acadian domains (Avalonia and Meguma) at depths < 120 km also have a NE-SW orientation. The low-velocity anomalies beneath Ganderia and the Peri-Gondwanan terranes in the Dunnage zone show a dominant NE-SW orientation at depths in the 100–140 km range. Figure 10 shows cross-sections of the model, oriented parallel and perpendicular to the Appalachian trend. This illustration clearly shows the complexity of velocity structure in the uppermost mantle across the study

area, especially beneath the Peri-Gondwanan domains (eastern parts of Dunnage zone, Ganderia, Avalonia, Meguma). We observe a less complex uppermost mantle structure in the Peri-Laurentian domains.

Teleseismic surface wave tomography studies are typically laterally smoothed. However, our checkerboard resolution tests suggest that our tomographic models are capable of recovering anomalies of at least 160 km in horizontal dimensions (Figure 6). This allows us to investigate patterns of seismic wave velocities across various accretionary domains. The low-velocity anomaly in the southern part of the study area, located beneath the GMA, is the largest and the strongest negative anomaly recovered in our study region. This anomaly is bounded by fast anomalies to its north-to-northeast and west with a significant velocity contrast of 3%–4% at a wide range of depths in our model (60–200 km; Figures 9 and 10). This suggests a significant decrease in seismic velocities toward the continental margin. The same low-velocity feature was also recovered in the previous continental-scale shear wave velocity model of Yuan et al. (2014), but starting to appear at a deeper depth (~100 km).

We notice in our tomography models that the boundary between Meguma and Avalonia is not clearly distinguishable. Avalonia and Ganderia show distinct seismic velocity signatures, and this is especially evident across the GSL, where the inversion results suggest a deeper Moho interface beneath Avalonia than Ganderia (Figure 9). A thinner Ganderia crust compared to the crustal thickness beneath Avalonia is also reported by previous studies (Chian et al., 1998; Figure 3 of C. Li et al., 2018; van Staal & Barr, 2012). Investigating our shear wave velocity model at lithospheric depths (~50–120 km), a generally faster and thicker lithosphere is suggested beneath Avalonia compared to Ganderia beneath the GSL. The presence of Avalonia lithosphere under the Ganderia domain at the deepest lithospheric depths is also suggested beneath GSL and the farthest southwest regions of our model. The observed geometry of the high-velocity anomalies beneath the southeastern GSL and eastern PEI supports this theory. Moreover, a high-velocity anomaly in the southwesternmost part of the study area is clearly visible beneath the coastline. As previous studies also placed the corresponding surface geological units into the Avalonian category (e.g., Hibbard et al., 2007a), we interpret this model feature as a piece of lithosphere belonging to Avalonia. Despite being a relatively small anomalous feature that is surrounded by slow anomalies, the continued appearance of this feature at depths <140 km and further validation provided by our resolution analysis (Figure 6) reinforce our interpretation of this anomaly and its geometry as a well-resolved feature.

Among the lithotectonic domains in the northern Appalachians, the uppermost mantle velocity structure of Ganderia and eastern Dunnage zone at lithospheric depths is mostly dominated by slower velocities, an exception being the distinctive, fast anomaly in New Brunswick (Section 6.3). We find the slow velocity anomaly in the southwestern study area spatially coinciding with the location of the North Appalachian Anomaly (NAA) also reported in previous studies (e.g., Menke et al., 2016). This slow anomaly is observable in the middle of cross-sections B26 and B28 (Figure 10). Although it is located at the edge of the confidence area, our resolution analysis indicates that the geometry of this anomaly is well recovered. It is very likely that we recovered a portion of this anomaly, and the main bulk of NAA is actually located outside the confidence area. This low-velocity anomaly becomes progressively weaker at depths below ~130 km in our model.

The seismic structure of the uppermost mantle at depths <100 km beneath the Grenville orogen and its neighboring Peri-Laurentian domains (i.e., Humber margin and western Dunnage zone) is dominated by faster seismic velocities when compared to the reference models used in this study. Interestingly, the uppermost mantle velocity structure of the western and eastern domains of Dunnage zone is different. Our velocity models suggest that the eastern Dunnage zone has a similar seismic signature to Ganderia at uppermost mantle depths. The seismic velocities in the western Dunnage zone, however, suggest similarities to the seismic signature of the Humber zone. According to our models, it is very likely that the Grenville lithosphere extends beneath both the Humber zone and the western domain of the Dunnage zone (e.g., van der Velden et al., 2004; van Staal & Barr, 2012).

6.2. Lithospheric Thickness Variations

Rychert et al. (2005, 2007) used receiver function analysis to infer a sharp LAB at ~100 km depth beneath the southeasternmost part of our study area. Surface wave tomography techniques are insensitive to the sharpness of a vertical boundary due to the nature of depth sensitivity kernels. Even so, variations in LAB

depth are commonly inferred in surface wave tomography via the use of regionally consistent proxies for the transition from lithosphere to asthenosphere (Eaton et al., 2009). Among previously employed proxies is a deviation, usually +1%–2%, from a global reference model (e.g., Darbyshire et al., 2013; Frederiksen et al., 2001). Here, we employ the contour of +1.5% shear wave velocity perturbation from the (continental) AK135 global reference model as the criteria for locating the lithosphere base.

Lithospheric thickness beneath the Peri-Laurentian domains is not very variable when compared to other tectonic zones in our study area. The lithospheric signature in the southeast Grenville Province suggests the LAB beneath this area being located at ~100 km depth. Lithospheric seismic velocities beneath the Humber zone are similar to the western Dunnage zone, and we interpret an average lithospheric thickness of ~90 km across these areas.

Southwestern Ganderia in the northern Appalachians is dominated by slow velocities coinciding with the passage of the Great Meteor Hotspot (GMH; Sleep, 1990; Heaman & Kjarsgaard, 2000). Our seismic definition for LAB cannot be used to infer the lithospheric thickness in this region as velocities are consistently too slow. Thermochemical erosion associated with the passage of GMH, between 190 and 110 Ma, has likely altered the composition of the lower lithosphere, reducing seismic velocities and thus making it challenging to use tomography models to infer the LAB depth. Most of GSL in our models (northwestern GSL) is situated in the Ganderia domain, and we interpret an average lithospheric thickness of 70 km beneath this region. We interpret a 30 km thicker Avalonia lithosphere under the farthest southeastern part of GSL (cross-section B04 in Figure 10). The low velocities below 100 km depth beneath the northwestern GSL are likely caused by a hot asthenosphere that persists to depths beyond our model resolution (e.g., Goes et al., 2000). The fastest recovered feature in our shear wave velocity model crosscuts Ganderia over New Brunswick. The strength and shape of this anomaly suggest that the fastest and thickest lithosphere in the study area is located beneath this region, with the LAB situated at ~120 km depth. A thick lithosphere with an NW-SE orientation beneath this area is unusual compared to other regions of Ganderia and across the Avalonia-Ganderia boundary within the study area. This implies that a localized change in the nature of subduction is likely to have occurred causing lithospheric growth beneath New Brunswick (Section 6.3). The edge of composite Laurentia (at the SE margin of the Grenville province) had an irregular shape before accretion of Peri-Gondwanan blocks, and this explains the offset of terranes between Newfoundland and our study area (Stockmal et al., 1987). For the same reason, a localized change in the nature of subduction beneath New Brunswick is possible.

The LAB beneath Nova Scotia is located at ~100 km depth, similar to that beneath the oldest tectonic unit in our study area, the SE Grenville. Nova Scotia contains terranes belonging to the latest accreted tectonic zones, Avalonia and Meguma. As discussed above, highly variable LAB depths (70–120 km) are interpreted in the other Peri-Laurentian and Peri-Gondwanan domains (Humber, Dunnage, and Ganderia). As a result, we conclude that there is no simple relation between the age of the terranes and their lithospheric thickness in our study area.

6.3. Tectonic Implications

6.3.1. Response of the Lithosphere to Hotspot Tectonism

The most recent magmatism in our study area occurred during the passage of the GMH beneath the North American lithosphere. The scale of lithospheric modification associated with the GMH tectonism appears highly variable (e.g., Boyce et al., 2016; Villemaire et al., 2012). Our higher-resolution model allows us to observe smaller-scale variations in this anomaly, at the scale of the individual tectonic domains. We note that the anomaly is stronger and more pervasive beneath the western domain of Ganderia and the Dunnage zone than beneath the older Humber zone. The base of this slow anomaly reaches to maximum ~120 km depth beneath the Ganderia-Dunnage boundary in the SW of the study area. Similar to the discussion by Boyce et al. (2016) and Villemaire et al. (2012), this observation implies that the older Peri-Laurentian domains were likely to be less compositionally modified due to the hotspot tectonism than the younger Peri-Gondwanan domains. This could, in part, be due to a thinner existing lithosphere beneath the peri-Gondwanan terranes before hotspot tectonism, causing more hot material to deflect beneath these

areas (e.g., Sleep, 1997). Alternatively, variations in the composition of the lithosphere could cause a different response to the hotspot magmatism (e.g., Villemaire et al., 2012).

6.3.2. Evidence for Avalonian Flat-Slab Subduction

Accretion of the terranes to eastern Laurentia in the Paleozoic was accompanied by multiple episodes of subduction and collision (e.g., Hibbard et al., 2007a). The convergence of Avalonia with eastern North America in the late Silurian to early Devonian is associated with a flat-slab setting after the onset of collision (van Staal & Barr, 2012; van Staal et al., 2009; Wilson et al., 2017). Geochronological measurements on volcanic rocks in New Brunswick indicate two-stage magmatism at 422–419 Ma and 417–407 Ma (Wilson et al., 2017). These time periods coincide with the accretion of Avalonia to composite Laurentia. This type of bimodal age pattern is a known observation that is usually seen in a flat-slab setting (Coney & Reynolds, 1977; Humphreys et al., 2003), and is compatible with the inference of two-stage magmatic activity following subduction of the lithosphere beneath the Acadian seaway under Ganderia and the subsequent slab break off, similar to the processes inferred for Andean subduction cycles (e.g., Haschke et al., 2002). In addition, the adakitic volcanics in New Brunswick exhibit high La/Yb ratios and Sr enrichment, similar to those observed in Chilean adakites (Wilson et al., 2017, and references therein). This enrichment is associated with the temporary halt in volcanism during flat-slab subduction, where the asthenospheric wedge is displaced and/or suppressed (e.g., Haschke et al., 2002).

The relatively thick and fast lithosphere beneath New Brunswick may result from stacking of the Avalonia slab after flat subduction of Acadian lithosphere under Ganderia. To understand the type of subduction at the time of Avalonia accretion, we consider the parameters affecting the strain regime of the Avalonia and Ganderia plates. Four variables including convergence rate, slab age, absolute motion of the upper plate, and intermediate dip (dip from the trench to ~100 km depth) are the main factors that influence this strain (Jarrard, 1986). Among these variables, high convergence rate and fast trenchward movement of composite Laurentia at the time of accretion are documented. Evidence from paleomagnetic studies suggests that the Laurentian plate was moving to the south (present-day coordinates) at a high rate of ~8–10 cm/year at the time of Avalonia accretion (e.g., Figure 8 in van Staal et al. [1998]). The dip angle of a downgoing slab is a function of the slab descent and convergence rates. This relation is explained by $\theta = \arcsin\left(\frac{V_z}{V_0}\right)$, where V_Z and V_0 are the descent rate due to gravity (often known as slab pull) and the rate of convergence, respectively (Luyendyk, 1970). A very fast convergence rate could dominate the other subduction variables and cause a shallow subduction. Moreover, a young Acadian slab would be buoyant, and therefore less affected by slab pull. This would also contribute to lowering the angle of subduction of the Acadian seaway beneath Ganderia (e.g., English & Johnston, 2004).

The lithosphere beneath northern Maine shows faster wave speeds than other areas of the Laurentian margin (cross-section B16, Figure 10). The elevated seismic velocities in this region can also be seen in the previous continental-scale models (Bedle & van der Lee, 2009; Schaeffer & Lebedev, 2014; van der Lee & Frederiksen, 2005). This fast lithospheric lid is interpreted to be Grenville lithosphere extended beneath these regions and may have contributed to flattening of the subducting Avalonia plate. Fast trenchward movement of cratons can cause flattening of a subducting slab (e.g., Manea et al., 2012). This craton-induced suction model is compatible with the observed geometry of the thick lithosphere beneath New Brunswick and the fast lithosphere beneath northern Maine (Figure 11).

6.3.3. Tectonic Evolution of the Northern Appalachian Region

We integrate the evidence discussed above to explain the observed features in our models. The main focus of our interpretations is on the events that occurred after the Salinic orogeny (Figure 11). During the Acadian orogeny, accretion of Avalonia to composite Laurentia occurred at a very high convergence rate. As a result, lithosphere beneath the Acadian seaway situated between Avalonia and Ganderia was subducted under the more buoyant Ganderia with a low dipping angle. Water-bearing minerals initiated limited magmatism between 422 and 419 Ma. As the flattened slab advanced toward the older Grenville basement, the slab broke off, resulting in the early Devonian (417–407 Ma) arc-like volcanism and uplift in New Brunswick and Maine. We suggest the present-day relatively thick lithosphere beneath New Brunswick in Ganderia is actually the remnant of the subducted Avalonia lithosphere contributing to the observed lithospheric

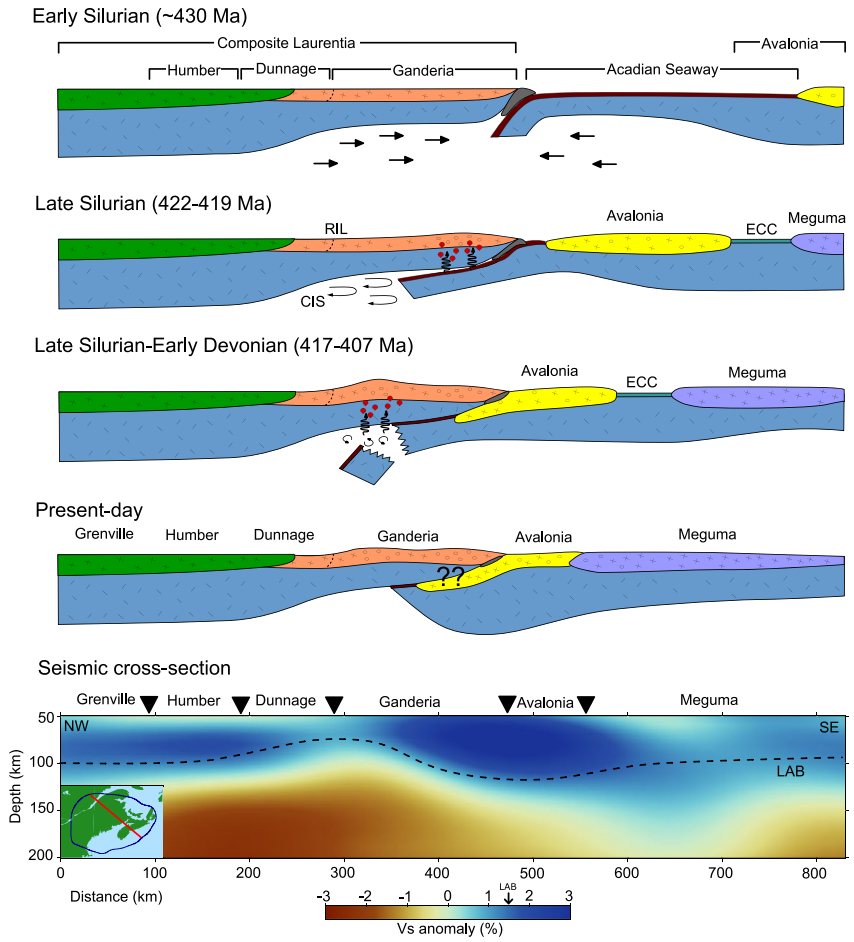

Figure 11. Tectonic history of the northern Appalachians and easternmost Grenville since the Early Silurian, modified from van Staal and Barr (2012). The inverted triangles in the seismic cross-section indicate the approximate present-day location of the tectonic boundaries at the surface. Our interpretation of the location of LAB is marked by the dashed line in the cross-section. The minimap at the lower left of the cross-section shows the location of the NW-SE profile (red line). CIS, craton-induced suction; ECC, extended continental crust; RIL, Red Indian Line.

thickness beneath this area. A similar interpretation, known as slab stacking, was previously suggested by other authors as a probable mechanism for lithospheric growth beneath cratons (Humphreys et al., 2015).

The thinner Ganderia crust beneath New Brunswick, where we interpret a stacked slab as a possible cause for the lithospheric growth, could be due to crustal destruction after the onset of Avalonia flat subduction beneath Ganderia. Crustal destruction could be accommodated by a number of processes, including sediment subduction, subduction erosion, and delamination (e.g., Brown, 2010; Scholl & von Huene, 2010). Although the amount of recycled crustal material in the past is unknown (Rino et al., 2004), the shallower Moho beneath New Brunswick may be a result of Ganderia crustal thinning associated with flat subduction.

Accretion of Meguma to Avalonia is associated with the subsequent events of the Neo-Acadian orogeny. It is not clear whether Meguma and Avalonia were separated by the Rheic oceanic lithosphere or by extended continental crust (e.g., van Staal & Barr, 2012). A lack of clear distinctive seismic signature across the Meguma-Avalonia boundary along with a relatively thick lithosphere beneath Nova Scotia favors the view that Avalonia and Meguma were in fact separated by thinned continental and/or transitional crust rather than Rheic oceanic lithosphere (Figure 11). If true, this means that what we see today is Meguma and Avalonia side by side directly, due to collision.

7. Conclusions

Eastern North America has been shaped by a series of tectonic events since the late Proterozoic. Our models provide us clues to answer some fundamental questions concerning these events. Using the highest resolution surface wave tomography models of the northern Appalachians and the southeast Grenville province to date, we show systematic variations of seismic velocities across different tectonic zones. The depth coverage of our shear wave velocity model covers uppermost mantle lithospheric and sub-lithospheric structures. Our models suggest less variable seismic signatures, including velocity and lithospheric thickness variations, beneath the Peri-Laurentian domains than the Peri-Gondwanan domains. An eastward decrease of the LAB depth is suggested in the Peri-Laurentian domains. However, our models do not suggest a simple relation between the age of different tectonic zones and the lithospheric thickness in the Peri-Gondwanan domains. A lack of distinct seismic signature at lithospheric depths beneath Avalonia and Meguma suggests that they were separated by a thinned continental and/or transitional crust rather than Rheic oceanic lithosphere. The LAB depth across the study area varies from 70 to 120 km, with more variabilities in the Peri-Gondwanan domains than the Peri-Laurentian domains. The lithosphere beneath older Ganderia is generally thinner than that beneath the younger Avalonia and Meguma domains. A thicker lithosphere beneath the New Brunswick part of Ganderia along with the NW-SE orientation of the corresponding positive anomaly suggests that a localized change in the nature of subduction of Avalonia under Ganderia may have occurred. We interpret the observed thicker lithosphere beneath that part of Ganderia as resulting from a slab stacking process after flat subduction of lithosphere beneath the Acadian seaway (Avalonia) in the late Silurian. Probable mechanisms to explain the flat subduction of Avalonia lithosphere beneath Ganderia include a fast convergence rate between the North American plate and the Avalonia block along with a cratonic-like Grenville basement at the time of accretion.

Data Availability Statement

The seismic data used in this study are archived at the IRIS Data Management Center (http://www.iris.edu/hq/; http://ds.iris.edu/ds/nodes/dmc/; networks (CN; Geological Survey of Canada, 1989), (NE; ASL, 1994), (TA; IRIS Transportable Array, 2003), (US; ASL/USGS, 1990), (X8, Y8; Menke et al., 2012; SEIS-UK, 2013)) or at the Canadian National Data Center, Natural Resources Canada (https://earthquakescanada.nrcan.gc.ca/stndon/index-en.php; CN; Geological Survey of Canada, 1989).

Acknowledgments
The authors thank the editor and reviewers for their helpful comments, which improved the manuscript. Aibing Li, Yingjie Yang, and their research groups are thanked for providing us the TPWT codes. The authors are thankful to the operators of the six networks used in this study. The authors also thank Andrew Schaeffer for providing the SL2013NA model. All figures in this study were generated using Generic Mapping Tools (Wessel et al., 2013) and python matplotlib library (Hunter, 2007). The scientific colormap of Crameri (2019) was used to illustrate the shear wave velocity model. The 3D topography and cross-section illustrations were rendered in Blender software (Blender Online Community, 2018). This study was supported by the Natural Sciences and Engineering Research Council of Canada (NSERC/CRSNG) through its Discovery Grant and Canada Research Chair programs.

References

Adams, A., Nyblade, A., & Weeraratne, D. (2012). Upper mantle shear wave velocity structure beneath the East African plateau: Evidence for a deep, plateauwide low velocity anomaly. *Geophysical Journal International*, *189*(1), 123–142. https://doi.org/10.1111/j.1365-246x.2012.05373.x

Artemieva, I. M. (2006). Global 1°×1° thermal model TC1 for the continental lithosphere: Implications for lithosphere secular evolution. *Tectonophysics*, *416*(1–4), 245–277. https://doi.org/10.1016/j.tecto.2005.11.022

ASL/USGS (1990). *United States National Seismic Network. International Federation of Digital Seismograph Networks. Dataset/Seismic Network*. https://doi.org/10.7914/SN/US

ASL. (1994). *New England Seismic Network. International Federation of Digital Seismograph Networks. Dataset/Seismic Network*. https://doi.org/10.7914/SN/NE

Bedle, H., & van der Lee, S. (2009). S velocity variations beneath North America. *Journal of Geophysical Research*, *114*(B7). https://doi.org/10.1029/2008JB005949

Blender Online Community. (2018). *Blender – A 3D modeling and rendering package [Computer software manual]*. Stichting Blender Foundation. Retrieved from http://www.blender.org

Boyce, A., Bastow, I. D., Darbyshire, F. A., Ellwood, A. G., Gilligan, A., Levin, V., & Menke, W. (2016). Subduction beneath Laurentia modified the eastern North American cratonic edge: Evidence from P wave and S wave tomography. *Journal of Geophysical Research: Solid Earth*, *121*(7), 5013–5030. https://doi.org/10.1002/2016JB012838

Boyce, A., Bastow, I. D., Golos, E. M., Rondenay, S., Burdick, S., & Van der Hilst, R. D. (2019). Variable modification of continental lithosphere during the Proterozoic Grenville orogeny: Evidence from teleseismic P-wave tomography. *Earth and Planetary Science Letters*, *525*, 115763. https://doi.org/10.1016/j.epsl.2019.115763

Brown, M. (2010). Melting of the continental crust during orogenesis: The thermal, rheological, and compositional consequences of melt transport from lower to upper continental crust. *Canadian Journal of Earth Sciences*, *47*(5), 655–694. https://doi.org/10.1139/E09-057

Calò, M., Bodin, T., & Romanowicz, B. (2016). Layered structure in the upper mantle across North America from joint inversion of long and short period seismic data. *Earth and Planetary Science Letters*, *449*, 164–175. https://doi.org/10.1016/j.epsl.2016.05.054

Chen, C.-W., & Li, A. (2012). Shear wave structure in the Grenville Province beneath the lower Great Lakes region from Rayleigh wave tomography. *Journal of Geophysical Research*, *117*(B1). https://doi.org/10.1029/2011JB008536

Chian, D., Marillier, F., Hall, J., & Quinlan, G. (1998). An improved velocity model for the crust and upper mantle along the central mobile belt of the Newfoundland Appalachian orogen and its offshore extension. *Canadian Journal of Earth Sciences*, *35*(11), 1238–1251. https://doi.org/10.1139/e98-042

Coney, P. J., & Reynolds, S. J. (1977). Cordilleran Benioff zones. *Nature*, *270*(5636), 403–406. https://doi.org/10.1038/270403a0

Cook, F. A., White, D. J., Jones, A. G., Eaton, D. W. S., Hall, J., & Clowes, R. M. (2010). How the crust meets the mantle: Lithoprobe perspectives on the Mohorovičić discontinuity and crust-mantle transition. *Canadian Journal of Earth Sciences*, *47*(4), 315–351. https://doi.org/10.1139/E09-076

Crameri, F. (2019). *Scientific color-maps (version 5.0.0)*. Zenodo. https://doi.org/10.5281/zenodo.3596401

Darbyshire, F. A., Bastow, I. D., Petrescu, L., Gilligan, A., & Thompson, D. A. (2017). A tale of two orogens: Crustal processes in the Proterozoic Trans-Hudson and Grenville Orogens, eastern Canada. *Tectonics*, *36*(8), 1633–1659. https://doi.org/10.1002/2017TC004479

Darbyshire, F. A., Eaton, D. W., & Bastow, I. D. (2013). Seismic imaging of the lithosphere beneath Hudson Bay: Episodic growth of the Laurentian mantle keel. *Earth and Planetary Science Letters*, *373*, 179–193. https://doi.org/10.1016/j.epsl.2013.05.002

Dorais, M. J., Atkinson, M., Kim, J., West, D. P., & Kirby, G. A. (2012). Where is the Iapetus suture in northern New England? A study of the Ammonoosuc Volcanics, Bronson Hill terrane, New Hampshire. *Canadian Journal of Earth Sciences*, *49*(1), 189–205. https://doi.org/10.1139/e10-108

Eaton, D. W., Darbyshire, F., Evans, R. L., Grütter, H., Jones, A. G., & Yuan, X. (2009). The elusive lithosphere-asthenosphere boundary (LAB) beneath cratons. *Lithos*, *109*(1–2), 1–22. https://doi.org/10.1016/j.lithos.2008.05.009

English, J. M., & Johnston, S. T. (2004). The Laramide orogeny: What were the driving forces?. *International Geology Review*, *46*(9), 833–838. https://doi.org/10.2747/0020-6814.46.9.833

Forsyth, D. W., & Li, A. (2005). Array analysis of two-dimensional variations in surface wave phase velocity and azimuthal anisotropy in the presence of multipathing interference. *Seismic Earth: Array Analysis of Broadband Seismograms*, *157*, 81–97. https://doi.org/10.1029/157GM06

Forsyth, D. W., Webb, S. C., Dorman, L. M., & Shen, Y. (1998). Phase velocities of Rayleigh waves in the MELT experiment on the East Pacific rise. *Science*, *280*(5367), 1235–1238. https://doi.org/10.1126/science.280.5367.1235

Frederiksen, A., Bostock, M., & Cassidy, J. (2001). S-wave velocity structure of the Canadian upper mantle. *Physics of the Earth and Planetary Interiors*, *124*(3–4), 175–191. https://doi.org/10.1016/S0031-9201(01)00194-7

Geological Survey of Canada. (1989). *Canadian National Seismograph Network. International Federation of Digital Seismograph Networks*. Dataset/Seismic Network. https://doi.org/10.7914/SN/CN

Goes, S., Govers, R., & Vacher, P. (2000). Shallow mantle temperatures under Europe from P and S wave tomography. *Journal of Geophysical Research*, *105*(B5), 11153–11169. https://doi.org/10.1029/1999JB900300

Golos, E. M., Fang, H., Yao, H., Zhang, H., Burdick, S., Vernon, F., et al. (2018). Shear wave tomography beneath the United States using a joint inversion of surface and body waves. *Journal of Geophysical Research: Solid Earth*, *123*(6), 5169–5189. https://doi.org/10.1029/2017JB014894

Haschke, M. R., Scheuber, E., Günther, A., & Reutter, K.-J. (2002). Evolutionary cycles during the Andean orogeny: Repeated slab breakoff and flat subduction?. *Terra Nova*, *14*(1), 49–55. https://doi.org/10.1046/j.1365-3121.2002.00387.x

Heaman, L., & Kjarsgaard, B. (2000). Timing of eastern North American kimberlite magmatism: Continental extension of the Great Meteor hotspot track?. *Earth and Planetary Science Letters*, *178*(3–4), 253–268. https://doi.org/10.1016/S0012-821X(00)00079-0

Herrmann, R. B. (2013). Computer programs in seismology: An evolving tool for instruction and research. *Seismological Research Letters*, *84*(6), 1081–1088. https://doi.org/10.1785/0220110096

Hibbard, J. P., van Staal, C. R., & Miller, B. V. (2007a). Links among Carolina, Avalonia, and Ganderia in the Appalachian peri-Gondwanan realm. *Geological Society of America Special Papers*, *433*, 291–311. https://doi.org/10.1130/2007.2433(1410.1130/2007.2433(14)

Hibbard, J. P., van Staal, C. R., & Rankin, D. W. (2007b). A comparative analysis of pre-Silurian crustal building blocks of the northern and the southern Appalachian orogen. *American Journal of Science*, *307*(1), 23–45. https://doi.org/10.2475/01.2007.02

Humphreys, E. D., Schmandt, B., Bezada, M. J., & Perry-Houts, J. (2015). Recent craton growth by slab stacking beneath Wyoming. *Earth and Planetary Science Letters*, *429*, 170–180. https://doi.org/10.1016/j.epsl.2015.07.066

Humphreys, E., Hessler, E., Dueker, K., Farmer, G. L., Erslev, E., & Atwater, T. (2003). How Laramide-age hydration of North American lithosphere by the Farallon slab controlled subsequent activity in the western United States. *International Geology Review*, *45*(7), 575–595. https://doi.org/10.2747/0020-6814.45.7.575

Hunter, J. D. (2007). Matplotlib: A 2D graphics environment. *Computing in Science & Engineering*, *9*(3), 90–95. https://doi.org/10.1109/MCSE.2007.55

Hynes, A., & Rivers, T. (2010). Protracted continental collision – Evidence from the Grenville orogen. *Canadian Journal of Earth Sciences*, *47*(5), 591–620. https://doi.org/10.1139/E10-003

IRIS Transportable Array. (2003). *USArray Transportable Array International Federation of Digital Seismograph Networks*. Dataset/Seismic Network. https://doi.org/10.7914/SN/TA

Jarrard, R. D. (1986). Relations among subduction parameters. *Reviews of Geophysics*, *24*(2), 217–284. https://doi.org/10.1029/RG024i002p00217

Kamo, S. L., Gower, C. F., & Krogh, T. E. (1989). Birthdate for the lapetus Ocean? A precise U-Pb zircon and baddeleyite age for the Long Range dikes, southeast Labrador. *Geology*, *17*(7), 602–605. https://doi.org/10.1130/0091-7613(1989)017⟨0602:BFTLOA⟩2.3.CO;210.1130/0091-7613(1989)017<0602:bftloa>2.3.co;2

Kao, H., Behr, Y., Currie, C. A., Hyndman, R., Townend, J., Lin, F.-C., et al. (2013). Ambient seismic noise tomography of Canada and adjacent regions: Part I. Crustal structures. *Journal of Geophysical Research: Solid Earth*, *118*(11), 5865–5887. https://doi.org/10.1002/2013JB010535

Kennett, B. L. N., Engdahl, E. R., & Buland, R. (1995). Constraints on seismic velocities in the Earth from traveltimes. *Geophysical Journal International*, *122*(1), 108–124. https://doi.org/10.1111/j.1365-246X.1995.tb03540.x

Kuponiyi, A. P., Kao, H., van Staal, C. R., Dosso, S. E., Cassidy, J. F., & Spence, G. D. (2017). Upper crustal investigation of the Gulf of Saint Lawrence region, eastern Canada using ambient noise tomography. *Journal of Geophysical Research: Solid Earth*, *122*(7), 5208–5227. https://doi.org/10.1002/2016JB013865

Levin, V., Servali, A., Van Tongeren, J., Menke, W., & Darbyshire, F. A. (2017). Crust-mantle boundary in eastern North America, from the (oldest) craton to the (youngest) rift. Geological Society of America Special Paper. https://doi.org/10.1130/2017.2526(06

Li, A. (2011). Shear wave model of southern Africa from regional Rayleigh wave tomography with 2-D sensitivity kernels. *Geophysical Journal International*, *185*(2), 832–844. https://doi.org/10.1111/j.1365-246X.2011.04971.x

Li, A., & Burke, K. (2006). Upper mantle structure of southern Africa from Rayleigh wave tomography. *Journal of Geophysical Research*, *111*(B10). https://doi.org/10.1029/2006jb004321

Li, A., & Detrick, R. S. (2006). Seismic structure of Iceland from Rayleigh wave inversions and geodynamic implications. *Earth and Planetary Science Letters*, *241*(3–4), 901–912. https://doi.org/10.1016/j.epsl.2005.10.031

Li, A., Forsyth, D. W., & Fischer, K. M. (2003). Shear velocity structure and azimuthal anisotropy beneath eastern North America from Rayleigh wave inversion. *Journal of Geophysical Research*, *108*(B8). https://doi.org/10.1029/2002JB002259

Li, A., & Li, L. (2015). Love wave tomography in southern Africa from a two-plane-wave inversion method. *Geophysical Journal International*, *202*(2), 1005–1020. https://doi.org/10.1093/gji/ggv203

Li, C., Gao, H., Williams, M. L., & Levin, V. (2018). Crustal thickness variation in the northern Appalachian Mountains: Implications for the geometry of 3-D tectonic boundaries within the crust. *Geophysical Research Letters*, *45*(12), 6061–6070. https://doi.org/10.1029/2018GL078777

Li, L., & Fu, Y. V. (2020). Surface-wave tomography of eastern and central Tibet from two-plane-wave inversion: Rayleigh-wave and love-wave phase velocity maps. *Bulletin of the Seismological Society of America*, *110*(3), 1359–1371. https://doi.org/10.1785/0120190199

Li, L., Li, A., Shen, Y., Sandvol, E. A., Shi, D., Li, H., & Li, X. (2013). Shear wave structure in the northeastern Tibetan Plateau from Rayleigh wave tomography. *Journal of Geophysical Research: Solid Earth*, *118*(8), 4170–4183. https://doi.org/10.1002/jgrb.50292

Luyendyk, B. P. (1970). Dips of downgoing lithospheric plates beneath island arcs. *Geological Society of America Bulletin*, *81*(11), 3411–3416. https://doi.org/10.1130/0016-7606(1970)81[3411:DODLPB]2.0.CO;2

Macdonald, F. A., Ryan-Davis, J., Coish, R. A., Crowley, J. L., & Karabinos, P. (2014). A newly identified Gondwanan terrane in the Northern Appalachian Mountains: Implications for the Taconic orogeny and closure of the Iapetus Ocean. *Geology*, *42*(6), 539–542. https://doi.org/10.1130/G35659.1

Manea, V. C., Pérez-Gussinyé, M., & Manea, M. (2012). Chilean flat slab subduction controlled by overriding plate thickness and trench rollback. *Geology*, *40*(1), 35–38. https://doi.org/10.1130/G32543.1

Menke, W., Levin, V., & Darbyshire, F. A. (2012). *Deep structure of three continental sutures in eastern North America (QM-III). International Federation of Digital Seismograph Networks. Dataset/Seismic Network*. https://doi.org/10.7914/SN/X8_2012

Menke, W., Skryzalin, P., Levin, V., Harper, T., Darbyshire, F., & Dong, T. (2016). The Northern Appalachian Anomaly: A modern asthenospheric upwelling. *Geophysical Research Letters*, *43*(19), 173–210. https://doi.org/10.1002/2016GL070

O'Donnell, J., Adams, A., Nyblade, A. A., Mulibo, G., & Tugume, F. (2013). The uppermost mantle shear wave velocity structure of eastern Africa from Rayleigh wave tomography: Constraints on rift evolution. *Geophysical Journal International*, *194*(2), 961–978. https://doi.org/10.1093/gji/ggt135

Pasyanos, M. E., Masters, T. G., Laske, G., & Ma, Z. (2014). LITHO1.0: An updated crust and lithospheric model of the Earth. *Journal of Geophysical Research: Solid Earth*, *119*(3), 2153–2173. https://doi.org/10.1002/2013JB010626

Petrescu, L., Darbyshire, F., Bastow, I., Totten, E., & Gilligan, A. (2017). Seismic anisotropy of Precambrian lithosphere: Insights from Rayleigh wave tomography of the eastern Superior Craton. *Journal of Geophysical Research: Solid Earth*, *122*(5), 3754–3775. https://doi.org/10.1002/2016JB013599

Priestley, K., McKenzie, D., & Ho, T. (2018). A lithosphere-asthenosphere boundary—A global model derived from multimode surface-wave tomography and petrology. *Lithospheric Discontinuities*, 111–123. https://doi.org/10.1002/9781119249740.ch6

Rino, S., Komiya, T., Windley, B. F., Katayama, I., Motoki, A., & Hirata, T. (2004). Major episodic increases of continental crustal growth determined from zircon ages of river sands: Implications for mantle overturns in the Early Precambrian. *Physics of the Earth and Planetary Interiors*, *146*(1–2), 369–394. https://doi.org/10.1016/j.pepi.2003.09.024

Ritzwoller, P., Macdonald, F. A., & Crowley, J. L. (2017). Bridging the gap between the foreland and hinterland I: Geochronology and plate tectonic geometry of Ordovician magmatism and terrane accretion on the Laurentian margin of New England. *American Journal of Science*, *317*(5), 515–554. https://doi.org/10.2475/05.2017.01

Rivers, T., Martignole, J., Gower, C. F., & Davidson, A. (1989). New tectonic divisions of the Grenville Province, southeast Canadian Shield. *Tectonics*, *8*(1), 63–84. https://doi.org/10.1029/TC008i001p00063

Rychert, C. A., Fischer, K. M., & Rondenay, S. (2005). A sharp lithosphere-asthenosphere boundary imaged beneath eastern North America. *Nature*, *436*(7050), 542–545. https://doi.org/10.1038/nature03904

Rychert, C. A., Rondenay, S., & Fischer, K. M. (2007). P-to-S and S-to-P imaging of a sharp lithosphere-asthenosphere boundary beneath eastern North America. *Journal of Geophysical Research*, *112*(B8). https://doi.org/10.1029/2006JB004619

Rychert, C. A., & Shearer, P. M. (2009). A global view of the lithosphere-asthenosphere boundary. *Science*, *324*(5926), 495–498. https://doi.org/10.1126/science.1169754

Saito, M. (1988). DISPER80: A subroutine package for the calculation of seismic normal-mode solutions. *Seismological Algorithms*, 293–319.

Schaeffer, A. J., & Lebedev, S. (2014). Imaging the North American continent using waveform inversion of global and USArray data. *Earth and Planetary Science Letters*, *402*, 26–41. https://doi.org/10.1016/j.epsl.2014.05.014

Schaeffer, P. T. C., Clowes, R. M., Cook, F. A., van der Velden, A. J., & Vasudevan, K. (2010). The Lithoprobe trans-continental lithospheric cross sections: Imaging the internal structure of the North American continent. *Canadian Journal of Earth Sciences*, *47*(5), 821–857. https://doi.org/10.1139/E10-036

Scholl, D. W., & von Huene, R. (2010). Subduction zone recycling processes and the rock record of crustal suture zones. *Canadian Journal of Earth Sciences*, *47*(5), 633–654. https://doi.org/10.1139/E09-061

SEIS-UK (2013). *QM-III Network – Atlantic Canada. International Federation of Digital Seismograph Networks.* Dataset/Seismic Network.

Sleep, N. H. (1990). Monteregian hotspot track: A long-lived mantle plume. *Journal of Geophysical Research*, *95*(B13), 21983–21990. https://doi.org/10.1029/JB095iB13p21983

Sleep, N. H. (1997). Lateral flow and ponding of starting plume material. *Journal of Geophysical Research*, *102*(B5), 10001–10012. https://doi.org/10.1029/97JB00551

Stockmal, G. S., Colman-Sadd, S. P., Keen, C. E., O'Brien, S. J., & Quinlan, G. (1987). Collision along an irregular margin: A regional plate tectonic interpretation of the Canadian Appalachians. *Canadian Journal of Earth Sciences*, *24*(6), 1098–1107. https://doi.org/10.1139/e87-107

van der Lee, S., & Frederiksen, A. (2005). Surface wave tomography applied to the North American upper mantle. *Seismic Earth: Array Analysis of Broadband Seismograms*, *157*, 67–80. https://doi.org/10.1029/157GM05

van der Velden, A. J., Van Staal, C. R., & Cook, F. A. (2004). Crustal structure, fossil subduction, and the tectonic evolution of the Newfoundland Appalachians: Evidence from a reprocessed seismic reflection survey. *The Geological Society of America Bulletin*, *116*(11–12), 1485–1498. https://doi.org/10.1130/B25518.1

van Staal, C. R., & Barr, S. (2012). Lithospheric architecture and tectonic evolution of the Canadian Appalachians and associated Atlantic margin. *Geological Association of Canada Special Paper*, *49*, 41–95.

van Staal, C. R., Barr, S. M., & Murphy, J. B. (2012). Provenance and tectonic evolution of Ganderia: Constraints on the evolution of the Iapetus and Rheic Oceans. *Geology*, *40*(11), 987–990. https://doi.org/10.1130/G33302.1

van Staal, C. R., Dewey, J. F., Niocaill, C. M., & McKerrow, W. S. (1998). The Cambrian-Silurian tectonic evolution of the northern Appalachians and British Caledonides: History of a complex, west and southwest Pacific-type segment of Iapetus. *Geological Society, London, Special Publications*, *143*(1), 197–242. https://doi.org/10.1144/GSL.SP.1998.143.01.17

van Staal, C. R., Whalen, J. B., Valverde-Vaquero, P., Zagorevski, A., & Rogers, N. (2009). Pre-carboniferous, episodic accretion-related, orogenesis along the Laurentian margin of the northern Appalachians. *Geological Society, London, Special Publications*, *327*(1), 271–316. https://doi.org/10.1144/SP327.13

Villemaire, M., Darbyshire, F. A., & Bastow, I. D. (2012). P-wave tomography of eastern North America: Evidence for mantle evolution from Archean to Phanerozoic, and modification during subsequent hot spot tectonism. *Journal of Geophysical Research*, *117*(B12), https://doi.org/10.1029/2012JB009639

Weeraratne, D. S., Forsyth, D. W., Fischer, K. M., & Nyblade, A. A. (2003). Evidence for an upper mantle plume beneath the Tanzanian craton from Rayleigh wave tomography. *Journal of Geophysical Research*, *108*(B9). https://doi.org/10.1029/2002jb002273

Wessel, P., Smith, W. H. F., Scharroo, R., Luis, J., & Wobbe, F. (2013). Generic mapping tools: Improved version released. *Eos, Transactions, American Geophysical Union*, *94*(45), 409–410. https://doi.org/10.1002/2013EO450001

Whitmeyer, S., & Karlstrom, K. E. (2007). Tectonic model for the Proterozoic growth of North America. *Geosphere*, *3*(4), 220–259. https://doi.org/10.1130/GES00055.1

Williams, H. (1979). Appalachian orogen in Canada. *Canadian Journal of Earth Sciences*, *16*, 792–807. https://doi.org/10.1139/e79-070

Williams, H., Colman-Sadd, S., & Swinden, H. (1988). *Tectonic-stratigraphic subdivisions of central Newfoundland. Current Research, Part B*. Geological Survey of Canada, Paper. https://doi.org/10.4095/122414

Wilson, R. A., van Staal, C. R., & Kamo, S. L. (2017). Rapid transition from the Salinic to Acadian orogenic cycles in the northern Appalachian Orogen: Evidence from northern New Brunswick, Canada. *American Journal of Science*, *317*(4), 449–482. https://doi.org/10.2475/04.2017.02

Yang, Y., & Forsyth, D. W. (2006). Regional tomographic inversion of the amplitude and phase of Rayleigh waves with 2-D sensitivity kernels. *Geophysical Journal International*, *166*(3), 1148–1160. https://doi.org/10.1111/j.1365-246X.2006.02972.x

Yuan, H., French, S., Cupillard, P., & Romanowicz, B. (2014). Lithospheric expression of geological units in central and eastern North America from full waveform tomography. *Earth and Planetary Science Letters*, *402*, 176–186. https://doi.org/10.1016/j.epsl.2013.11.057

Zhou, Y., Dahlen, F. A., & Nolet, G. (2004). Three-dimensional sensitivity kernels for surface wave observables. *Geophysical Journal International*, *158*(1), 142–168. https://doi.org/10.1111/j.1365-246X.2004.02324.x

Zhu, H., Yang, J., & Li, X. (2020). Azimuthal anisotropy of the North American upper mantle based on full waveform inversion. *Journal of Geophysical Research: Solid Earth*, *125*(2), e2019JB018432. https://doi.org/10.1029/2019JB018432